THERMAL COMFORT ANALYSIS OF MILITARY AIRCRAFT CABIN USING COMPUTATIONAL FLUID DYNAMICS

A THESIS SUBMITTED TO
THE GRADUATE SCHOOL OF NATURAL AND APPLIED SCIENCES
OF
MIDDLE EAST TECHNICAL UNIVERSITY

BY

İREM KÖSE

IN PARTIAL FULFILLMENT OF THE REQUIREMENTS
FOR
THE DEGREE OF MASTER OF SCIENCE
IN
MECHANICAL ENGINEERING

SEPTEMBER 2022

Approval of the thesis:

THERMAL COMFORT ANALYSIS OF MILITARY AIRCRAFT CABIN USING COMPUTATIONAL FLUID DYNAMICS

submitted by **İREM KÖSE** in partial fulfillment of the requirements for the degree of **Master of Science** i**n Mechanical Engineering, Middle East Technical University** by,

Prof. Dr. Halil KALIPÇILAR
Dean, Graduate School of **Natural and Applied Sciences** _____

Prof. Dr. M. A. Sahir Arıkan
Head of the Department, **Mechanical Engineering** _____

Prof. Dr. M. Metin Yavuz
Supervisor, **Mechanical Engineering, METU** _____

Examining Committee Members:

Prof. Dr. Cüneyt Sert
Mechanical Eng, METU _____

Prof. Dr. M. Metin Yavuz
Mechanical Eng, METU _____

Prof. Dr. Murat Aktaş
Mechanical Eng, TOBB ETU _____

Asst. Prof. Dr. Özgür Uğraş Baran
Mechanical Eng, METU _____

Asst. Prof. Dr. Ali Karakuş
Mechanical Eng, METU _____

Date: 01.09.2022

I hereby declare that all information in this document has been obtained and presented in accordance with academic rules and ethical conduct. I also declare that, as required by these rules and conduct, I have fully cited and referenced all material and results that are not original to this work.

Name Last name: İrem Köse

Signature:

ABSTRACT

THERMAL COMFORT ANALYSIS OF MILITARY AIRCRAFT CABIN USING COMPUTATIONAL FLUID DYNAMICS

Köse, İrem
Master of Science, Mechanical Engineering
Supervisor: Prof. Dr. M. Metin Yavuz

September 2022, 88 pages

Thermal comfort is essential for human health and welfare during aircraft operations. In military aircraft, these thermal problems are getting more difficult because of the high-altitude operations, cockpit transparency, mission flights, pilot clothing, and an increasing amount of mission equipment. Therefore, supplying the correct amount of cooling air into the cockpit, good air distribution around the occupants, and keeping the other thermal comfort measurements at a satisfactory level in the cockpit significantly impacts pilots' thermal comfort.

In this study, the thermal comfort of pilots in the cockpit is aimed to be developed with the help of thermal comfort measures and CFD modeling. During the evaluation, general thermal comfort parameters have been defined and assessed with the standards (JSSG-2009, SAE-ARP-85F, and MIL-E-18927E). Then, a suitable CFD turbulence model was chosen for the analyses, and it was validated with the numerical and experimental results given in the literature. With the performance model generation, the cockpit air distribution model was evaluated with the help of thermal comfort measures. According to the results, old-type piccolo air inlet models have been found insufficient to provide comfortable conditions to the occupant. Therefore, a more newly used version of the air inlet, which provides jet flow to the

cabin, and foot inlet have been evaluated, and it was found more efficient than the piccolo-type air inlets. In addition, foot inlets influenced the air distribution around the cockpit positively. As a result of this study, evaluating the comfort with general parameters is not enough to compare the thermal conditions. However, the positive effect of changing the inlet type from piccolo to gasper and adding foot inlets has been observed.

Keywords: CFD Modelling, Thermal Comfort, Piccolo inlet, Gasper inlet, WBGT

ÖZ

ASKERİ UÇAK KABİNİNİN HESAPLAMALI AKIŞKANLAR DİNAMİĞİ KULLANILARAK TERMAL KONFOR ANALİZİ

Köse, İrem
Yüksek Lisans, Makina Mühendisliği
Tez Yöneticisi: Prof. Dr. M. Metin Yavuz

Eylül 2022, 88 Sayfa

Uçuş operasyonlarında, termal konfor insan sağlığı ve konforu için büyük önem taşımaktadır. Yüksek irtifa uçuşları, kokpit ışık geçirgenliği, görev uçuşları, pilot kıyafetleri ve görev sistemi ekipmanlarındaki sayıca artış sebebiyle, bu durum savaş uçaklarında termal konfor sorununu daha zorlu hale getirmektedir. Bu nedenle, kokpit içerisine doğru miktarda soğuk havanın sağlanması, kokpit içerisindeki düzgün hava dağılımı ve diğer termal konfor ölçüm parametrelerini belirli bir memnuniyet seviyesinde tutmanın, pilotun termal konforu üzerinde büyük bir etkisi bulunmaktadır.

Bu çalışmada, pilotun kokpit içerisindeki termal konforunun çeşitli termal konfor ölçüm yöntemlerinin ve hesaplamalı akışkanlar dinamiğinin yardımıyla modellemesi ve geliştirilmesi hedeflenmiştir. Değerlendirme esnasında genel termal konfor parametreleri tanımlanmış ve standartlar yardımıyla değerlendirilmiştir (JSSG-2009, SAE-ARP-85F ve MIL-E-18927E). Daha sonra uygun türbülans modellemesi seçilmiş ve literatürde bulunan nümerik ve deneysel sonuçlarla doğrulanmıştır. Performans modelinin oluşturulmasıyla birlikte, kokpit içerisindeki hava dağılımı termal konfor ölçüm yöntemleriyle değerlendirilmiştir. Sonuçlara göre, eski tip

piccolo hava girişleri kullanıcıya yeterli konfor alanını sunamamıştır. Bu nedenle daha güncel bir hava giriş tipi olan, jet tipi hava giriş modeli ve ayak hava girişleri değerlendirilmiş ve picollo tipi hava girişlerinden daha verimli olduğu bulunmuştur. Ek olarak, ayak hava girişleri kokpit içerisindeki hava dağılımını olumlu etkilemiştir. Bu çalışmanın sonucunda, konforun genel parametrelerle değerlendirilmesinin termal konfor koşullarının karşılaştırılmasında yeterli olmadığı sonucuna varılmıştır. Ancak, hava girişlerinin piccolo'dan gasper'a çevrilmesinin ve ayak hava girişi eklenmesinin pozitif etkileri olduğu gözlemlenmiştir.

Anahtar Kelimeler: HAD Modelleme, Termal Konfor, Picollo hava girişi, Gasper hava girişi, YAKS

To: my family, my team, my best lecturer

ACKNOWLEDGMENTS

I would like to express my gratitude and respect to my best lecturer and supervisor, Prof. Dr. M. Metin Yavuz, and I would like to thank him for his guidance and leadership throughout the research.

My mother, Yasemin, my father, Süleyman, and my brother Mustafa Mert is always supporting me to achieve everything that I dream of throughout my life. Therefore, I couldn’t succeed without their support.

My Turkish Aerospace team's technical guidance and moral support are also gratefully acknowledged.

TABLE OF CONTENTS

LIST OF TABLES

TABLES

LIST OF FIGURES

FIGURES

LIST OF ABBREVIATIONS

ASHRAE	American Society of Heating, Refrigerating and Air-Conditioning Engineers
CEAS	Council of European Aerospace Societies
CET	Corrected Effective Temperature
CFD	Computational Fluid Dynamics
DBT	Dry Bulb Temperature
DES	Detached Eddy Simulation
ECS	Environmental Control System
ET	Effective Temperature
FITS	Fighter Index of Thermal Stress
GT	Globe Temperature
ISA	International Standard Atmosphere
ISO	International Organization for Standardization
JSSG	The Joint Service Specification Guides
LES	Large Eddy Simulation

MD	Mcdonnell Douglas
NATO	North Atlantic Treaty Organization
NBC	Nuclear Biological Chemical
PET	Pilot Envelope Temperature
PIV	Particle Image Velocimetry
PMV	Predicted Mean Vote
PPD	Predicted Percentage of Dissatisfied
PV	Personalized Ventilation
RANS	Reynolds Averaged Navier Stokes
RNG	Renormalization Group
SAAB	Svenska Aeroplan Aktie Bolag
SAE	Society of Automotive Engineers
STANAG	Standardization Agreement
TSR	Tactical Strike and Reconnaissance

WBGT	Wet Bulb Globe Temperature
WBT	Wet Bulb Temperature

LIST OF SYMBOLS

Q_M	Metabolic Rate (W)
Q_R	Radiation (W)
Q_{Conv}	Convection (W)
Q_{Evap}	Evaporative Heat Loss from the human (W)
ΔQ_S	Stored Energy in the occupant (W)
A_D	De Bois Surface Area (m^2)
m	Mass of a human body (kg)
h	Height of a human body (m)
I_{clo}	Clothing Insulation (clo)
T_{PE}	Pilot Envelope Temperature (°C)
T_{out}	Cabin Outlet Air Temperature (°C)
T_{in}	Cabin Inlet Air Temperature (°C)
T_{WB}	Wet Bulb Temperature (°C)
T_G	Globe Temperature (°C)

T_{DB}	Dry Bulb Temperature (°C)
$\dot{q}_M$	Metabolic Rate (W/m^2)
q_{TL}	Thermal Load (W)
q_H	Metabolic Heat (W)
q_{diff}	Diffusive heat through the skin to clothes (W)
q_{rsw}	Evaporative cooling with sweating (W)
q_L	Heat loss with respiration (W)
q_R	Radiative heat transfer (W)
q_C	Convective heat transfer (W)
$u(t)$	Instantaneous velocity
$\bar{u}$	Mean velocity
u'	Fluctuating velocity
φ	General Flow Parameter
t	Time

u	x-velocity
v	y-velocity
p	Pressure
μ_t	Eddy viscosity (turbulent viscosity)
k	Turbulent kinetic energy per unit mass
δ_{ij}	Kronecker delta
ε	Rate of viscous dissipation
C_μ	Empirical constant
y^+	A non-dimensionless distance
U^+	A non-dimensionless velocity

CHAPTER 1

INTRODUCTION

The nature of a human being requires thermally stable and limited conditions to keep its comfort. Therefore, thermal comfort is highly demanding in different industries with developing technology.

Today, fast industrial development increases the power consumption rates of electronics, and these high demands affect the thermal conditions of the environment. As a result, it requires rising cooling rates. In addition, the growing living standards push the suppliers to design high-quality cooling systems. Therefore, manufacturers give more importance to thermal comfort with time.

In the aircraft industry, the same demand is also available, but in military aircraft, it has different opportunities for the pilot. Since the fighter pilots face more challenging conditions during the flights, developing better thermal conditions provides less stress for the pilots in mission operations.

1.1 The Aim of Study

Thermal comfort is a subjective term, but some general factors are same for most people. Therefore, common standard definitions are specified for thermal comfort. This thesis aims to define the thermal comfort of the military aircraft pilot and the development of the cooling system installations with the help of air inlet types used in history. For this study, different cooling inlet types were investigated, and their effects on the cockpit air distribution were evaluated. In addition, other thermal comfort measures have been used since the thermal comfort conditions are not only related to cooling air temperature and velocities.

1.2 Structure of the Thesis

The thesis has been created from five different chapters. The first chapter mentions the study's primary aim, the thesis statement's general view, and the literature review of the thesis. Then, the historical development of thermal comfort was detailed, and similar studies done up to today have been investigated. In addition, three primary purposes have been aimed in this chapter. Firstly, the definition of thermal comfort has been explained with the help of different resources. Secondly, the motivation of this study has been given, and then thermal comfort measures have been described.

In Chapter 2, the theoretical and mathematical background of the turbulence modeling of this thesis has been explained. Then, the chosen test case to evaluate the turbulence modeling of this thesis has been assessed. The geometrical modeling, mesh independence study, and turbulence modeling of the case with almost similar thermal and geometrical conditions have been done and reviewed. Finally, the performance of the chosen test case has been examined.

In Chapter 3, the primary thesis case condition has been modeled according to military aircraft geometry. Then, the mesh independence of the thesis case has been acknowledged. Finally, the solution has been observed and the thermal comfort condition has been evaluated with the help of thermal comfort measures.

In Chapter 4, the observed data from the previous section has been compared with the new geometrical shape and number of inlets. In addition, thermal comfort measures have been used to compare these two different inlet types of aircraft.

In Chapter 5, the conclusion and the possible future works of study have been given.

1.3 Literature Search

In today's world, the aircraft industry is the most demanded means of transportation with increasing living standards. [1]. Therefore, airlines give importance to passengers' thermal comfort and health while purchasing aircraft. [2] After the 2020 Global Pandemic, the importance of air distribution over passengers has increased, and investigations about the air distribution over passengers have widened significantly. Until today, many aircraft manufacturers and institutions have performed excellently to improve passenger comfort and well-being [1].
In this part of the thesis, the investigations about thermal comfort have been described, and suitable turbulence models used for the thermal comfort CFD calculations have been defined.

1.3.1 Thermal Comfort and Air-Distribution CFD Studies

When the literature is reviewed, many studies are conducted to investigate the air distribution around humans and the thermal comfort conditions of the environment. Different industries require this information, such as construction, transportation, and space. Therefore, mainly aircraft and similar vehicle studies have been referenced to define the best CFD model and detect the suitable thermal comfort conditions for this research. Almost the past ten years of studies have been referred to during the investigation.

When the historical timeline was reviewed, Shen and Yuan [3] used the human model to evaluate the air and heat distribution around a fighter pilot in the military aircraft cockpit. The experimental and numerical methods are used to verify the thermal comfort of the pilot, and they have resulted that the human model they used in their study is convenient for defining the occupant's thermal comfort. They observed that the realizable k-ε model is suitable for thermal comfort calculations compared with the experimental data during the investigation.

In another research, Liu et al. [4] studied three different turbulence models to evaluate flow distribution in the cabin of MD-82 commercial aircraft, which are RNG k-ε, DES, and LES. They analyzed both the empty and the occupied cabin, and as a result of the study, RNG k-ε has been found convenient for the occupied one. However, DES and LES have given good results for both cabin conditions. They have detailly given the human body heat distribution during the occupied cabin conditions as shown in Table 1.3.1-1.

Table 1.3.1-1 Heat Distribution Percentages adopted from Liu et.al. [4]

Body Segments	**Heat Generated by Thermal Manikin (W)**	**Percentage (%)**
Head and Neck	5.7	7.6
Trunk	20.1	26.8
Left Arm	8.2	10.9
Right Arm	8.2	10.9
Left Leg	16.4	21.9
Right Leg	16.4	21.9
Total	75.0	100.0

Again, Liu et al. [5] published another article to show all the studies done on the air distribution of aircraft cabins in terms of thermal comfort and cabin health conditions. According to the study, it is seen that CFD models are almost efficient in detecting the correct air distribution in the aircraft. The studies about the flow distributions in aircraft cabins have been given in Figure 1.3-1.

Author(s)	Year	Cabin	Manikins	Tech(s)	Data	CFD
Aboosaidi et.al.	1991	A cabin mock--up	None	N/A	V	RANS
Olander and Westlin	1991	DC 9-21, DC 9-41 and MD-80's	Passengers	N/A	V, C	Zonal Model
Mizuno and Warfield	1992	A cabin mock--up	None	HW, GS	V, C	RANS
Müller et.al.	1997	A340	N/A	PTV	V	RANS
Singh et.al.	2002	B737 mockup	Heated Cylinders	PSV	V, T	RANS
Mo et.al.	2003	B737	A thermal manikin and heated cylinders	PIV	V	None
Garner et.al.	2004	B747-100	None	UA	V	An augmented laminar Taylor-stabilized finite turbulent model
Wang et.al.	2005	B767 mockup	Thermal Manikins	VPTV	V	None
Sun et.al.	2005	B767 mockup	Thermal Manikins	VPSV	V	None
Lin et.al.	2005	B767	Human-shape manikins	V,	C	RANS/LES
Zhang et.al.	2005	B767 mockup	Box manikins	None	V, T, C	RNG k-ε
Bosbach et.al.	2006	A380	None	PIV	V	RANS
Lin et.al.	2006	Half of a generic empty cabin mockup	None	PIV	V	LES
Günther et.al.	2006	A380 mockup	None	PIV	V	RANS
Baker et.al.	2006	B747	None	SA	V	RANS
Zhang and Chen	2007	B767 mockup	Box manikins	None	V, T, C	RNG k-ε
Kühn et.al.	2008	A380 mockup	Thermal Manikins	OIV, TC	V, T	None
Yan et.al.	2008	B767 mockup	Box manikins	VPTV, GS	V, C	Standard k-ε
Zhang et.al.	2008	B767 mockup	Box manikins	UA, GS	V, C, T	RNG k-ε
Mazumdar and Chen	2008	B767 mockup	Box manikins	UA, GS	V, C	RNG k-ε
Wang et.al.	2008	B767 mockup	Thermal Manikins	VPTV, GS	V, C	None
Sze et.al.	2009	Cabin mockup	Heated Cylinders	PIV	V, C	None
Wan et.al.	2009	Cabin mockup	Heated Cylinders	PIV	V, C	RNG k-ε
Yin et.al.	2009	B767 mockup	Box manikins	None	V, T, C	RNG k-ε
Bianco et.al.	2009	Executive aircraft cabin	None	None	V, T	RANS
Bosbach et.al.	2009	A380 mockup	Thermal Manikins	PIV	V	None
Rosenstiel et.al.	2010	Full-scale cabin mockup	Heated dummies	PSV	V	None
Poussou et.al.	2010	Small-scale, water-filled model	Box manikins	PIV, PLIF	V, C	RNG k-ε
Dygert et.al.	2010	B767	Thermal Manikins	N/A	V, T, C	Realizable k-ε
Zítek et.al.	2010	B767 mockup	Box manikins	PIV	V, T	Standard k-ε

Figure 1.3-1 Air Distribution Studies in Airline Cabins up to 2011 adopted from [5]

After reviewing similar vehicles, a study by Ningbai [6] evaluated air distribution in hybrid electrical vehicles. The study aimed to optimize the air distribution contour in the vehicle with the conservation of energy efficiency. During the investigation, various turbulence models are evaluated with the experimental data, and the realizable k-ε model has been selected to be convenient for accuracy.

Again, Liu et al. [7] investigated a particular study to reduce the number of CFD analyses. For this study, they have used the PMV method, which will be mentioned in the following sections of this thesis, combined with the CFD model. As a result of the study, they have observed the best input conditions with the small amount of analysis run with the k-ε turbulence model.

Although several CFD studies are done for the thermal comfort of the occupants, some studies give input to these CFD studies. For example, Johansson E. [8] conducted a study with SAAB pilots and used thermal comfort measures like PMV

and PPD to evaluate the well-being of the occupants. According to the experimental results and measurements, it has resulted that when these techniques are detailed with each thermal comfort factor which will be defined in the following sections, predictions about the thermal comfort of the pilots become more reliable.

When we return to CFD air distribution studies, Pang et al. [9] studied the effect of the cabin's interior design on air distribution over the occupants. They have solved two different cabin ceiling designs for B737-800 commercial aircraft with the RNG k-ε turbulence model. During the study, they used the PMV method for objectivity. As a result of the study, they have observed that the cabin's design significantly impacts the occupants. Therefore, an air distribution system should be designed for each cabin with different orientations. Şahin D. [10] also evaluated the cabin air distribution of the newly designed helicopter. The air inlet locations and flow rates were modified to obtain the most suitable thermal conditions for the crew in this study. The k-ε turbulence model is also used in the study.

Finally, Jia Z. et al. [11] investigated a numerical optimization study to control the flow distribution around the fighter aircraft cockpit with the help of Fluent. The weighted average temperature calculation method has been used to confirm the optimized temperature around the cockpit. During the same time frame, Ali et al. [12] also conducted a study to investigate the effect of the moving occupant in the cabin on thermal conditions. The observations taken from the k-ε turbulence modeled CFD domain have been compared with the experimental results from the Airbus A380 aircraft.

According to all research, almost all use the k-ε turbulence model since it is cheap and straightforward for these calculations. RNG k-ε is also good at near-wall boundary conditions and is preferred in the literature. After reviewing the literature, a general approach to thermal comfort CFD analyses has been acknowledged.

1.4 Thermal Comfort Evaluation Methods

Thermal comfort is a problem for industrial sectors like automotive, aerospace, and construction. Therefore, the definition of thermal comfort is essential for cooling/heating system designs.

1.4.1 Definition of Thermal Comfort

Two main standardization tools can be referred to for this study: The International Organization for Standardization (ISO) and The American Society of Heating, Refrigerating and Air-Conditioning Engineers (ASHRAE). Both standardization societies apply to each sector. Therefore, these two standardizations have been used to define thermal comfort at first.

According to ISO 7730:2006, *thermal comfort* is a satisfying condition in a thermal environment. [13] When it comes to ASHRAE 55 Standard, this definition becomes a subjective condition with the summation of different environments where the person feels themself in physical and mental comfort [14]. As a result of these definitions, it is understood that thermal comfort is a subjective phenomenon. Therefore, the factors that affect thermal comfort have been investigated. According to the research, three main factors have been defined that affect on thermal comfort of the human body, as shown in Table 1.4.1-1. These environmental, personal, and contributing factors can change from person to person. Unless a unique design is requested, environmental factors are the main factors for the environmental control systems. Since personal and contributing factors are mainly subjective, designing the system according to these factors can make the system over-qualified. Therefore, environmental factors are the main factors for developing air-conditioning systems.

Table 1.4.1-1 Thermal Comfort Factors [16]

Environmental	Personal	Contributing Factors
Air Temperature	Metabolic Rate	Food and Drink
Air Movement (Velocity)	Clothing	Acclimatization
Humidity		Body Shape
Radiation		Subcutaneous fat
		Age and Gender
		State of health

In this thesis study, *environmental factors* have been defined as the main factors for thermal comfort. However, since the aerospace industry has different challenges in terms of thermal comfort and also military aircraft have more challenging thermal problems like:

- The high-altitude operations,
- Cockpit transparency,
- Mission flight,
- Pilot clothing,
- Increasing amount of mission equipment,

There is a detailed study required for this thesis. According to these factors, a comprehensive research about thermal comfort has been performed to define suitable thermal comfort measurement parameters.

A couple of thermal comfort measurement indices have been defined in the literature. When some of them are summarized, there is a diagram created as given below:

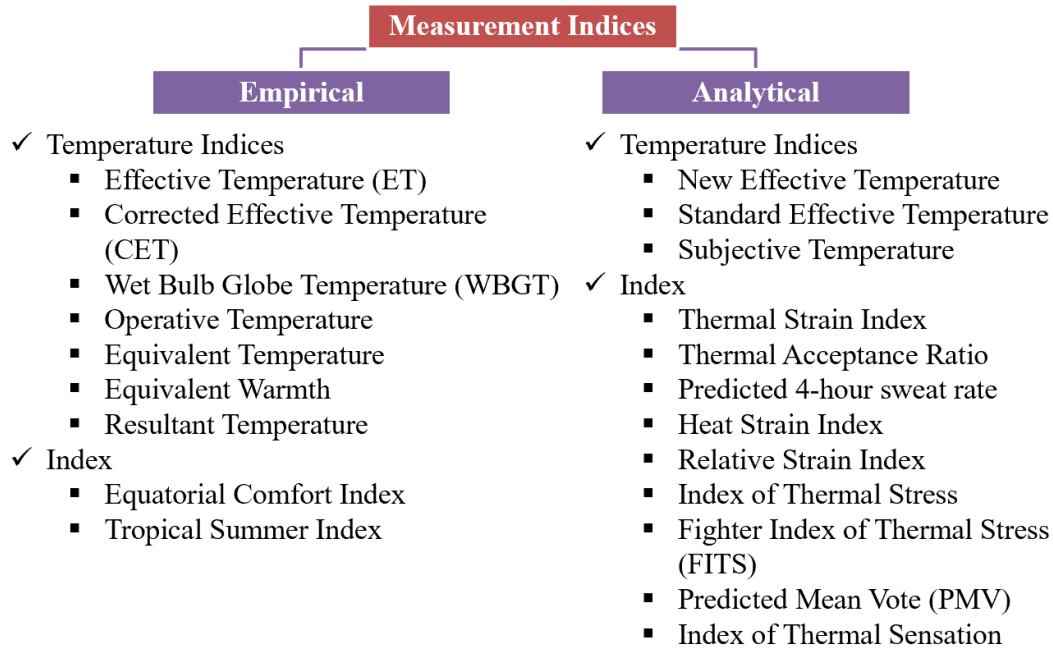

Figure 1.4-1- Thermal Comfort Measures (This diagram has been created according to the information defined in [16])

Each thermal comfort measure has a different approach regarding the factors affecting human well-being and related acclimatization found in the location where the analysis is done. Before giving the details of these measures, the primary motivation and the criteria defined in the aerospace industry for thermal comfort have been described in Section 1.4.2.

1.4.2 Motivation of the Thesis Study

There are different kinds of standards for military aircraft designs. For this study, some basic standards have been used to define the main criteria for designing the input variables and CFD analysis results. The requirements for the analysis are taken from these standards. The standards used in the study are as given below:

1. JSSG 2009: Military Specification Environmental Control Systems, Aircraft General Requirements [17]
2. MIL-E-18927E Military Specification Environmental Control Systems, Aircraft General Requirements [18]
3. DEF-STAN 00-970 Section 4: Ministry of Defense-Defense Standard [20]
4. SAE-ARP-85F: Air-Conditioning Systems for Subsonic Airplanes [19]

Since this study aims to evaluate the possible air-distribution system's effects on the thermal comfort of the fighter pilot, the primary inputs that will be used in the study have been detailed with these standards' recommendations.

The first primary input is the air inlets of the cockpit. The requirement defined in JSSG-2009 has been used to determine the number of inlet air gaspers or ducts. The requirement suggests that at least two air inlets are required per occupant. If possible, this number of channels should be increased, two of the inlets should be directed to the face side of the pilot, and the other two should be directed to the lateral parts of the occupant. The example air inlet positions for F5 aircraft have been given in Figure 1.4-2.

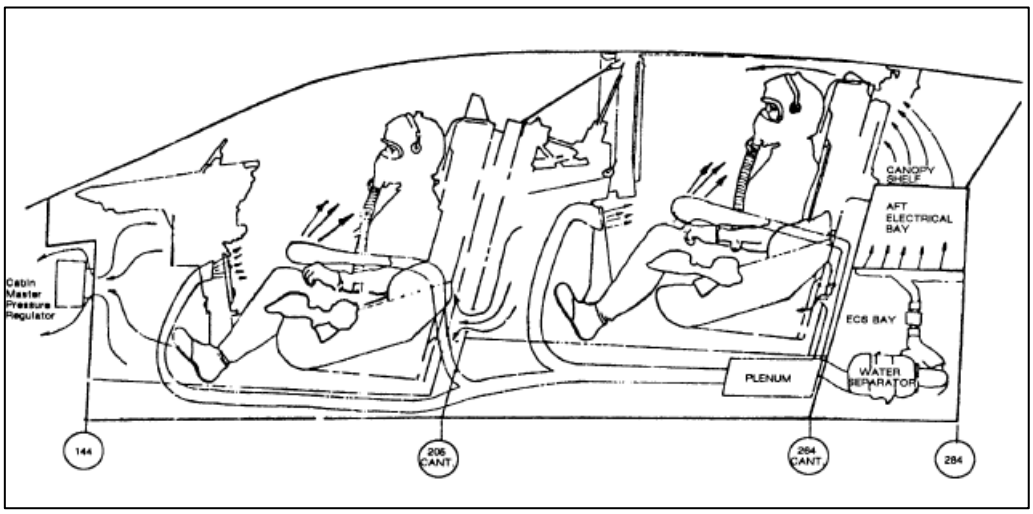

Figure 1.4-2- F-5F Air Distribution System Schematic [17]

The temperature that enters the cockpit is also limited to 2°C as a recommendation by SAE-ARP-85F. [19] The upper limit of this inlet temperature is 71°C. Since the case evaluated in this thesis is the cooling conditions, the minimum limit will be the input for the analysis. In addition, providing air to the cockpit at 2°C is ideal; therefore, the insulation should be considered to be applied to cooling system ducts.

Secondly, the temperature distribution around the cockpit is highlighted in the standards. The temperature differences between the pilot's head and foot levels are suggested to be kept at 2.8°C in JSSG-2009 [17] and SAE-ARP-85F [19]. This difference kept the pilot's thermal comfort at a certain healthy level. The other suggested requirement for the condition of the air around the pilot is the air velocity around the pilot's head. It is recommended that this jet air velocity value should be kept at a minimum of 1 m/s, but the general air velocity should not be most than 0.3 m/s by SAE-ARP-85F [19].

Finally, according to the experiments and verifications that have been done for other aircraft, JSSG-2009 [17] suggests that the exhaust air temperature from the cockpit should not exceed 35°C. In addition, the standard approach for the pilot's thermal comfort is to keep the crew's average skin temperature at 33°C [20] since this is the common thermal comfort condition that almost all thermal comfort indices reach at

the end. However, different kinds of thermal comfort indices were developed easily to find and define the correct level, as shown in Figure 1.4-1.

1.4.3 Thermal Comfort Measures

There are different kinds of measures developed by other researchers up to today. The first heat balance calculation model was suggested by Gagge (1936) [16]. According to his proposition, the heat balance model of the human being is:

$$Q_M \pm Q_R \pm Q_{Conv} \pm Q_{Cond} - Q_{Evap} = \Delta Q_S \qquad (1.4\text{-}1)$$

Q_M: Metabolic Rate (W)

Q_R: Radiation (W)

Q_{Conv}: Convection (W)

Q_{Cond}: Conduction (W)

Q_{Evap}: Evaporative Heat Loss from the human (W)

ΔQ_S: Stored Energy in the occupant (W) (According to the sign of this parameter, body temperature is increasing or decreasing [16])

The schematic of the heat balance model is given in Figure 1.4-3.

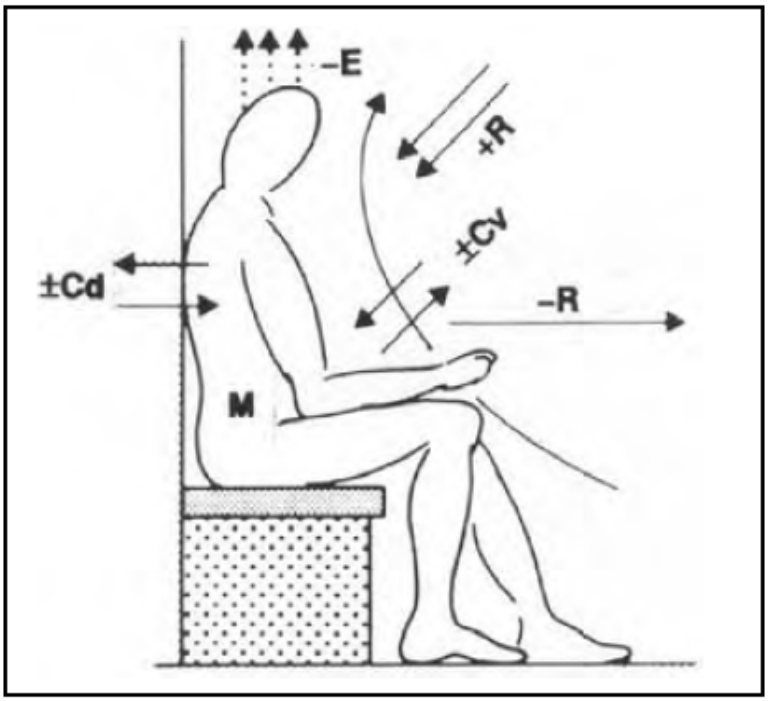

Figure 1.4-3 Heat balance model of a typical seated human being [16]

According to this model, besides the available heat sources, metabolism and conduction are specific essential factors for thermal comfort. Therefore, these two factors have been researched in detail. Firstly, the metabolic rate has been investigated for the CFD analysis. From ASHRAE 55 Standard [14], the fighter aircraft pilot's metabolic heat has been defined as given in Table 1.4.3-1

Table 1.4.3-1 Metabolic Rates for Different Activities [14]

Activity	**Met Units**	**W/m2**	**Btu/h.ft2**
Driving/ Flying			
Automobile	1.0-2.0	60-115	18-37
Aircraft, routine	1.2	70	22
Aircraft, instrument landing	1.8	105	33
Aircraft, combat	2.4	140	44
Heavy vehicle	3.2	185	59

Another reference has also been used to ensure the typical fighter pilot's metabolic rate. In [21], it is stated that the average in-flight metabolic rate has been defined between 100 kcal/hr to 225 kcal/hr. When typical pilot dimensions have been considered, the surface area of the human body has been calculated with Du Bois's (1916) [16] formula as given below:

$$A_D = 0.202 * m^{0.425} * h^{0.725} \quad (1.4\text{-}2)$$

A_D: De Bois Surface Area (m^2)

m: Mass of a human body (kg)

h: Height of a human body (m)

A 30-year-old man with 70 kg, 175 cm → 1.85 m^2

The metabolic rate of a typical pilot becomes:

$$\frac{225\ kcal/hr}{1.85\ m^2} = 121.62\ \frac{kcal}{hr * m^2} = \boxed{140.72\ \frac{W}{m^2}}$$

As a result of these references, the metabolic rate for a typical combat pilot has been defined as ~140 W/m^2.

In addition to metabolic rate, conduction is crucial for thermal comfort, and it is understood that the clothing and the seated area mainly cause it. Therefore, to define the effect of the clothing, there is detailed research done on the typical combat pilots. Again two different sources have been used to determine the impact of the clothing. In Johansson E. (2017) [8], typical pilot clothing components' insulations have been defined. With the help of these inputs from ASHRAE 55, there is an equation defined by McCullough and Jones to calculate the overall clothing insulation of the person in 1984:

$$I_{clo} = 0.835 * \sum_i I_{clo,i} + 0.161\ clo \quad (1.4\text{-}3)$$

(1 clo =0.155 m^2.K/W)

Before calculating the overall clothing insulation effect, an interview was done with the Turkish test pilots. Each component used for a typical combat pilot has been defined for winter, summer, and mission flight conditions. According to these inputs, the clothing effect has been described. In addition, as mentioned before, sitting is also causing thermal heat over the occupant. For this issue, ASHRAE 55 [14] has suggested adding 0.15 clo to the overall clothing insulation to simulate the seat effect.

After these specific factors have also been considered, the measures applicable for military aircraft have been investigated. Finally, the indices below have been defined to be evaluated in the thesis.

1.4.3.1 Pilot Envelope Temperature (PET)

Pilot Envelope Temperature is a typical temperature calculation method in most standards like JSSG 2009, SAE-ARP-85F, and MIL-E-18927E. It is the combination of the outlet and the inlet temperatures of the airflow. Dry bulb temperatures of these boundaries are used in the formulation. It is an acceptable approach to detect the thermal comfort of pilots easily. The related formulation of PET:

$$T_{PE} = 0.85 * T_{out} + 0.15 * T_{in} \qquad (1.4\text{-}4)$$

T_{PE}: Pilot Envelope Temperature

T_{out}: Cabin Outlet Air Temperature

T_{in}: Cabin Inlet Air Temperature

The temperature limits defined for Pilot Envelope Temperature to keep the comfort of the pilot at certain limits have been described in DEF-STAN, MIL-E-18927E are as given in Figure 1.4-4.

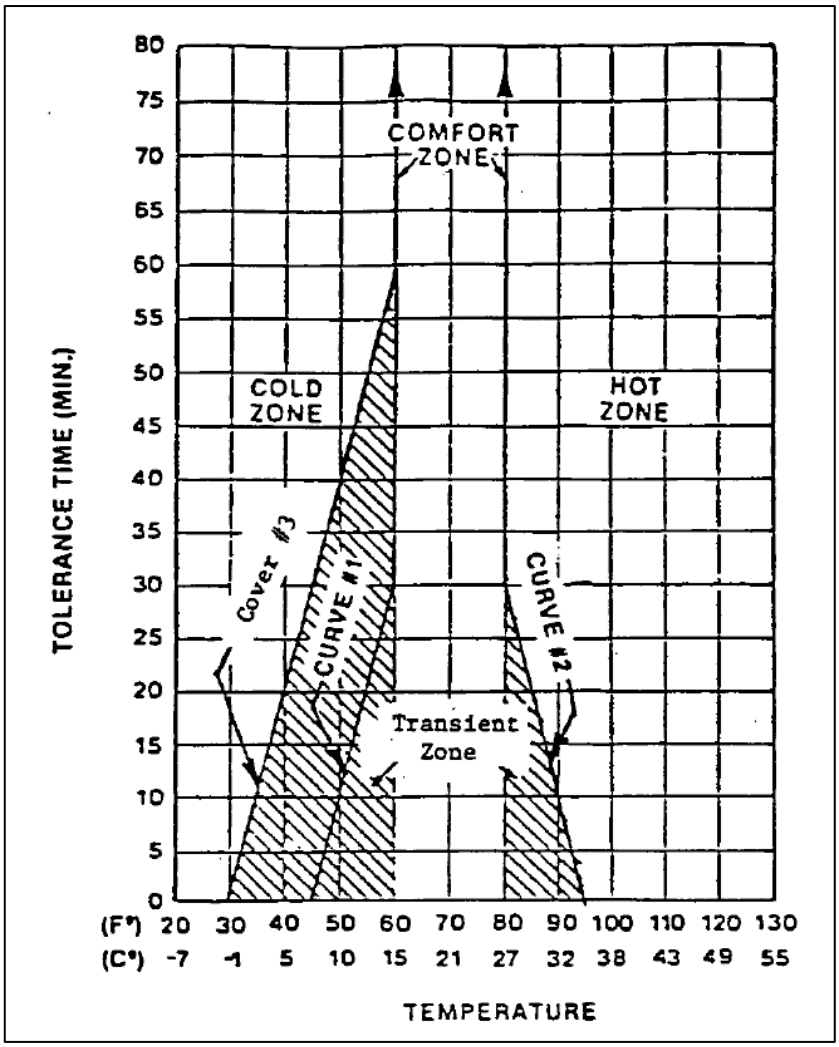

Figure 1.4-4 Thermal comfort limits for occupied compartments [18]

1.4.3.2 Wet Bulb Globe Temperature (WBGT)

WBGT (Wet Bulb Globe Temperature) has been mentioned in most military aerospace standards and journals like JSSG 2009, MIL-E-18927E, DEF-STAN 00-970, CEAS Aeronautical Journal, etc. This temperature is the combination of the dry bulb, wet bulb, global temperatures, and the air velocity for outdoor applications as given in the equation:

$$WBGT = 0.7 * T_{WB} + 0.2 * T_G + 0.1 * T_{DB} \quad (1.4\text{-}5)$$

T_{WB}: Wet Bulb Temperature

T_G: Globe Temperature

T_{DB}: Dry Bulb Temperature

Humidity, air temperature, and radiation effects can directly be understood from this temperature. However, a chart has been developed to understand the metabolic impact, as given in Figure 1.4-5. [16]

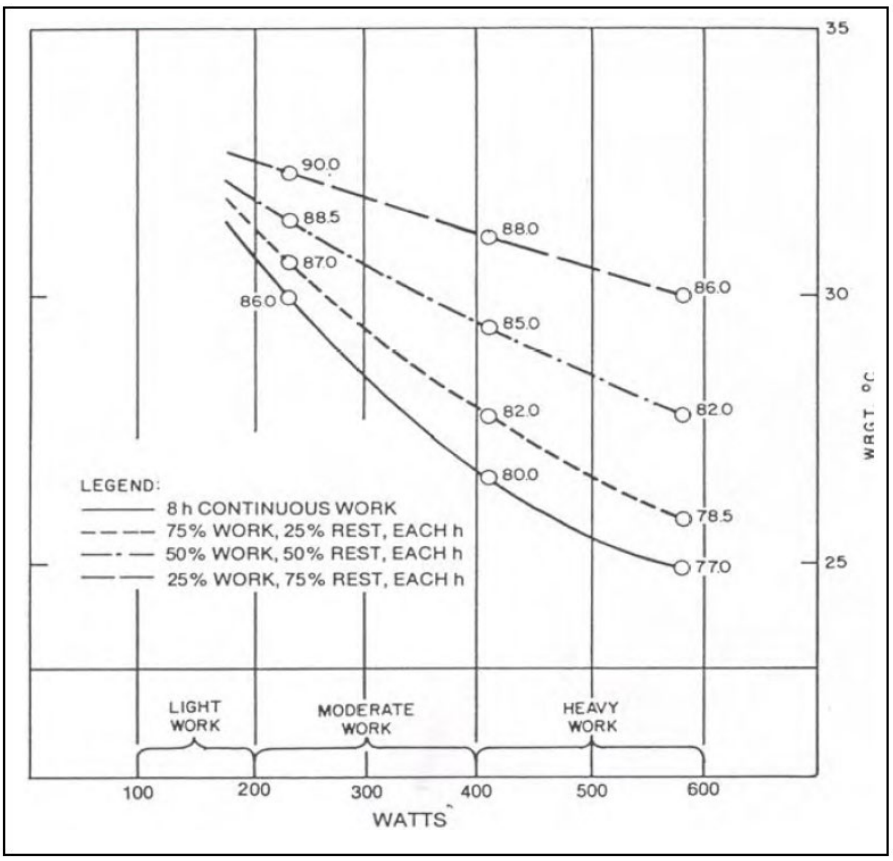

Figure 1.4-5 Metabolic Heat Transfer Limits with related WBGT [16]

In addition to the metabolic effect, in [22], the clothing effect has been considered to understand how it thermally affects WBGT. A related impact of this insulation will be mentioned in Section 3.3.

The temperature limits for the pilot thermal comfort with WBGT have been defined differently in different sources. According to CEAS [23], the target temperature to keep the occupant's skin temperature at 33°C, which is the comfort limit, is 28°C WBGT. In MIL-E-18927E, this exposure limit has been defined as 32°C for flight operations and 35°C for ground operations. In JSSG 2009, it is mentioned that 32°C WBGT has been used in Air Force.

1.4.3.3 Predicted Mean Vote (PMV)

Rather than WBGT and PET, this is not a temperature calculation for thermal comfort. It uses ASHRAE thermal comfort ranges to express the human thermal limits [16]. This index has already included all of the thermal comfort factors in itself. It combines typical energy balance equations with zero storage which refers to Fanger's heat balance equation. When all of the parameters are combined in a particular formulation, the short version of the PMV equation is:

$$PMV = \left[0.352 * e^{\left(-0.042\frac{\dot{q}_M}{A_D}\right)} + 0.032\right] * q_{TL} \quad (1.4\text{-}6)$$

PMV: Predicted Mean Vote

$\dot{q}_M$: Metabolic Rate (W/m^2)

A_D: De Bois Area (m^2)

q_{TL}: Thermal Load (W)

$$q_{TL} = q_H - q_{diff} - q_{rsw} - q_L - q_R - q_C \quad (1.4\text{-}7)$$

q_H: Metabolic Heat (W)

q_{diff}: Diffusive heat through the skin to clothes (W)

q_{rsw}: Evaporative cooling with sweating (W)

q_L: Heat loss with respiration (W)

q_R: Radiative heat transfer (W)

q_C: Convective heat transfer (W)

This index is evaluated with the PMV-PPD chart defined in [16] as given in Figure 1.4-6. According to the calculated data, PMV offers a comfortable condition of this index for the occupant.

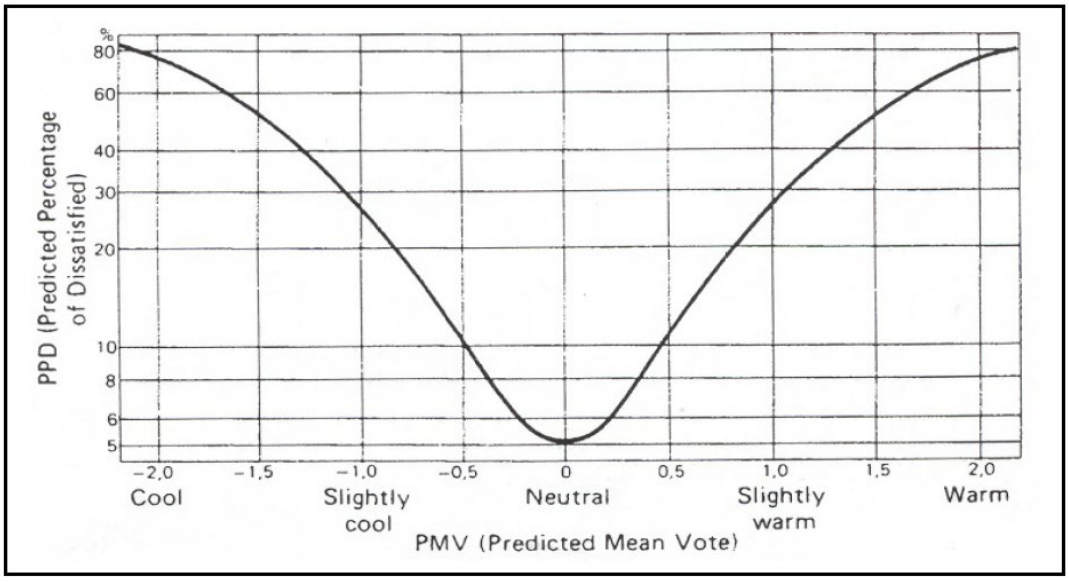

Figure 1.4-6- PMV-PPD Diagram [16]

CHAPTER 2

TURBULENCE MODELING

In Computational Fluid Dynamics (CFD), in addition to general conservation equations, turbulence modeling is also important to be solved to obtain correct results from the problem domain. Since capturing the eddies in turbulent flows are complex and expensive, turbulence modeling techniques have been used to determine the turbulent flow. In this thesis, since it is the most common and easy-to-use one, Reynolds Averaged Navier-Stokes (RANS) model has been used. There are a couple of approaches in RANS models.

2.1 Reynolds Decomposition

Turbulent flows are related to random, irregular, and rotational flow structures. The flow is defined as the composition of mean and fluctuating flow components to determine the flow structures meaningfully. Thus, Reynolds decomposition methods have been developed.

$$u(t) = \bar{u} + u' \tag{2-1}$$

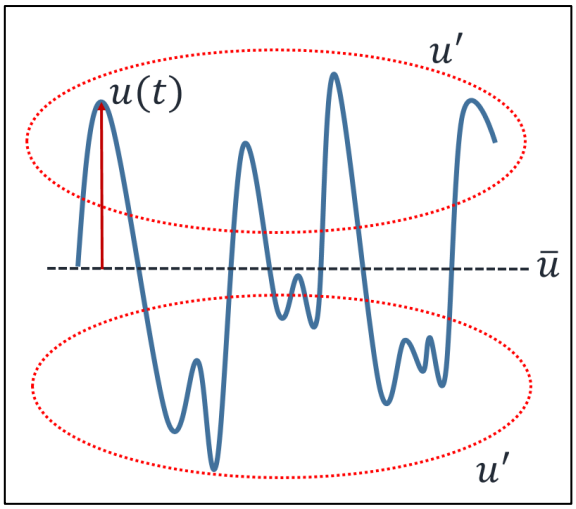

Figure 2.1-1 Reynolds Decomposition Representation of Velocity

General flow variables have also been defined from mean and fluctuating parts, and these new variables have been implemented into conservation equations.

$$\varphi(t) = \bar{\varphi} + \varphi' \tag{2-2}$$

φ: general flow parameter

$$\bar{\varphi} = \frac{\int_t^{t+\Delta t} \varphi dt}{\Delta t} \tag{2-3}$$

The continuity equation for 2D flow becomes:

$$\frac{\partial u}{\partial x} + \frac{\partial v}{\partial y} = 0 \rightarrow \frac{\partial \bar{u}}{\partial x} + \frac{\partial \bar{v}}{\partial y} = 0 \tag{2-4}$$

Momentum Equations for 2D flow become:

$$\frac{\partial(\rho\bar{u})}{\partial t} + \nabla \cdot \left(\rho\bar{u}\vec{\bar{V}}\right) = -\frac{\partial \bar{p}}{\partial x} + \nabla \cdot (\mu \nabla \bar{u}) + \nabla \cdot (-\rho\overline{u'\vec{V'}}) \tag{2-5}$$

$$\frac{\partial(\rho\bar{v})}{\partial t} + \nabla \cdot \left(\rho\bar{v}\vec{\bar{V}}\right) = -\frac{\partial \bar{p}}{\partial y} + \nabla \cdot (\mu \nabla \bar{v}) + \nabla \cdot (-\rho\overline{v'\vec{V'}})$$

Second moment of velocity fluctuations

Although the mean of the fluctuating terms is zero, the second moment of these terms is not. Therefore, these additional terms found in the equations cause Reynolds Stresses. They require special attention to be solved.

For 3D problem calculations, four equations and ten unknowns have been found. Since there are more unknowns than the equations, a certain simplification is required. To solve this problem, Boussinesq Analogy has been proposed.

2.1.1 Boussinesq Analogy

To easily solve the equations defined in RANS models, there is an approximation proposed by Boussinesq in 1877 [24]. In the Boussinesq analogy, the turbulent eddies have been proposed to be modeled with viscous eddies. For incompressible flow, this relationship becomes

$$-\rho\overline{V_i'V_j'} = \mu_t\left(\frac{\partial V_i}{\partial x_j}+\frac{\partial V_j}{\partial x_i}\right)-\frac{2}{3}\rho k\delta_{ij} \qquad (2\text{-}6)$$

μ_t: Eddy viscosity (turbulent viscosity)

k: Turbulent kinetic energy per unit mass ($k=\frac{1}{2}(\overline{u'^2}+\overline{v'^2}$)

δ_{ij}: Kronecker delta

This approximation method decreases the number of six Reynolds Stress variables to one flow property μ_t. After the number of variables has been reduced, then the molecular viscosity requires to be solved. To solve this variable, there are different kinds of turbulence models have been developed:

- Spalart-Allmaras
- Baldwin-Lomax
- k-ε Model
- k-ω Model

2.1.2 k-ε Turbulence Model

k-ε Model is the oldest, most common, and tested RANS model [37]. several studies have been done in the literature to solve the cockpit domains for thermal comfort CFD modeling. It is a two-equation method to solve eddy viscosity, μ_t.

There are two additional equations with the variables of k and ε (rate of viscous dissipation) that used to be solved with the leading conservation equations (continuity and momentum). These additional equations are obtained from several experimental studies. According to the calculations done, eddy viscosity becomes:

$$u_t = \frac{\rho C_\mu k^2}{\varepsilon} \tag{2-7}$$

C_μ: empirical constant

There are some different versions of the k- ε model available in the literature like Standard k- ε, RNG k- ε, and Realizable k- ε. Each one implies more physics into the models. The differences between these models are the improved predictions among each other for different kinds of problem domains [26].

2.1.3 Near–Wall Treatment

In Finite Volume calculations, flow variables are solved linearly among the grids. However, in real-life cases, since the flow is not changing linearly at the wall boundaries, it is hard to capture the flow correctly in near-wall regions. Therefore, the wall shear stress has been modified to calculate the flow. Viscosity has been modified on grid faces for this modification.

After a couple of calculations have been defined in the literature using shear stress and velocity profiles. There is a general equation obtained as given below:

$$v_W = v(\frac{y^+}{f(y^+)}) \tag{2-8}$$

To specify this equation, Standard wall functions have been defined.

$$U^+ = f(y^+) = \begin{cases} y^+ & y^+ < 11.25 \\ \frac{1}{\kappa}\log(Ey^+) & y^+ > 11.25 \end{cases}$$

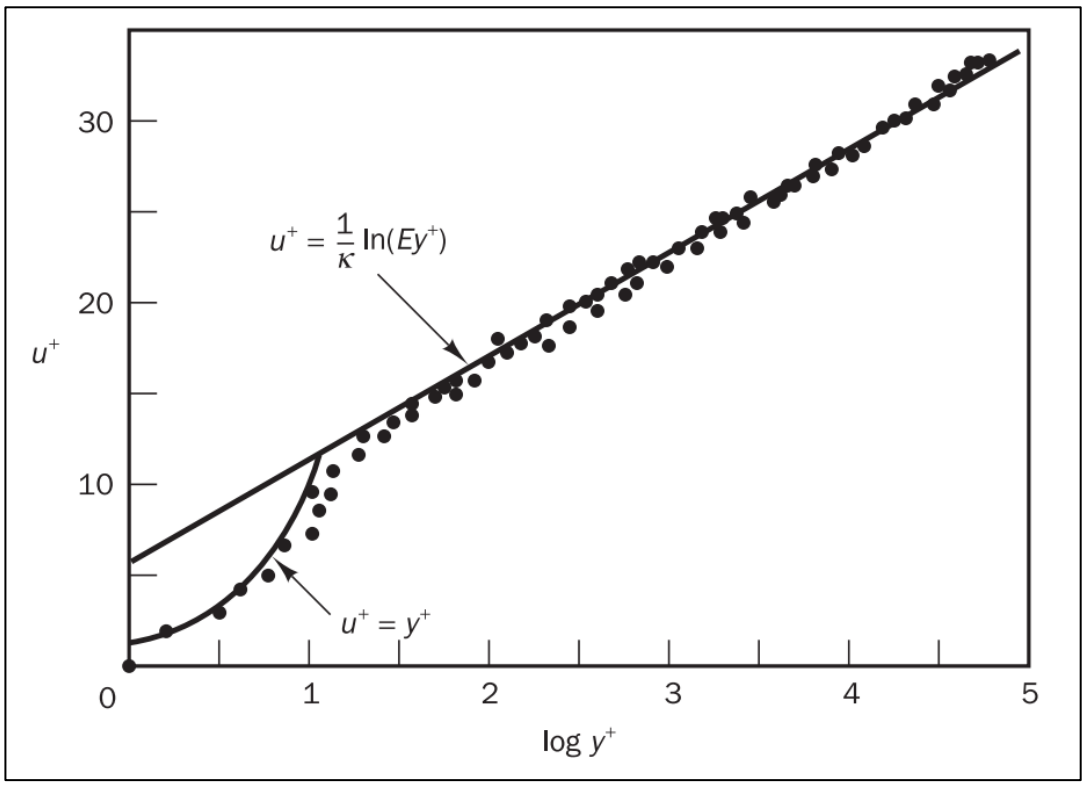

Figure 2.1-2 Velocity Distribution near the Wall boundary [25]

Since the profile is not linear, the values between 5 and 30 of y^+, calculation errors occur [26]. Therefore, in ANSYS Fluent, a particular wall function named "Enhanced Wall Function" has been developed to capture the flow near the wall. According to the Enhanced Wall Function method, $U^+=f(y^+)$ has been defined as:

$$f(y^+) = e^{\gamma}{u_{lam}}^+ + e^{1/\gamma}{u_{tur}}^+ \tag{2-9}$$

$$\gamma = \frac{-0.01(y^+)^4}{1+5y^+} \quad (2\text{-}10)$$

This new function approach captures the actual flow closer than the Standard Wall Function. Therefore, when a precise calculation is needed at the wall, the Enhanced Wall Function can be used to capture the flow. According to the Enhanced Wall Function, y^+ should be kept at less than 1 for the accuracy of the solution. However, for complex geometries, ANSYS Fluent guidance [26] gives a broader range of limitations for the calculations ($y^+<5$).

2.2 Turbulence Model Evaluation

This section of the thesis aims to evaluate the turbulence model for thermal comfort CFD analysis. During the benchmarking of the test case, a clear definition of the case, geometric dimensions, boundary condition information about the case, the relevancy with the main thesis study, up-to-dateness, and mesh independency were the primary concerns.

2.2.1 Test Case: Problem Description

For the test case of this thesis, Liu et al.'s [27]'s Boeing 737 commercial aircraft cabin model has been taken as a reference. In this study, Liu et al. [27] evaluated the turbulence models to simulate the air distribution in the passenger cabin. The article has also used experimental data from Particle Image Velocimetry (PIV) and Hot Wire Spherical Anemometers (HAS) to validate the results.

In the study, a human simulator is used to simulate the natural thermal effect of a typical commercial aircraft. The Personalized Ventilation (PV) [28] shown in Figure 2.2-1 is found in this aircraft. Therefore, fresh air is directed to the passenger with a gasper found over the occupant. This gasper solution helps to create personalized ventilation for the occupant.

In this Boeing 737 aircraft study, only half of the cabin has been taken as a control volume since the cabin is symmetric. Therefore, the experimental mock-up of the study has been built as half of the full-scale dimensions, which are 2.2 m in height (+z direction), 3.5 m in width (+x direction), and 0.9 m in depth (+y direction) given in Table 2.2.1-1 and Figure 2.2-2. This half cabin geometry helps to reduce the computational work.

Table 2.2.1-1- Single Aisle Aircraft Cabin Dimensions [27]

One-Row Single Aisle Cabin Mock-up Dimensions	
Width (x)	3.5 m
Depth (y)	0.9 m
Height (z)	2.2 m

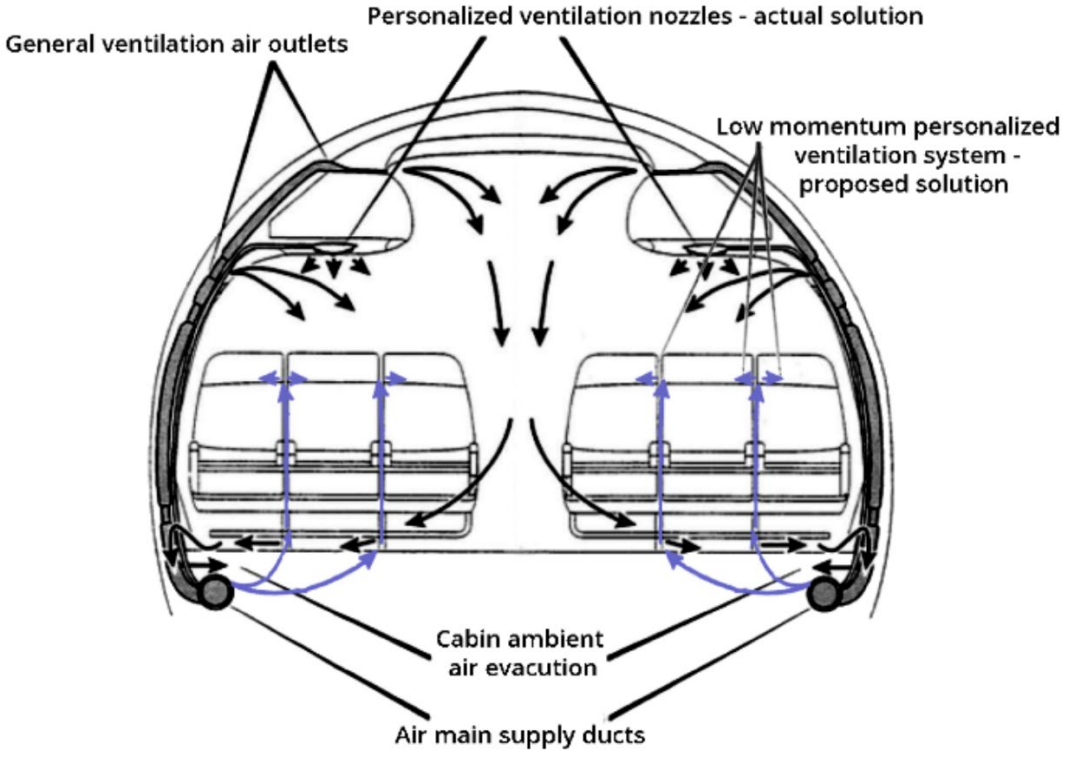

Figure 2.2-1- Personalized Ventilation [28]

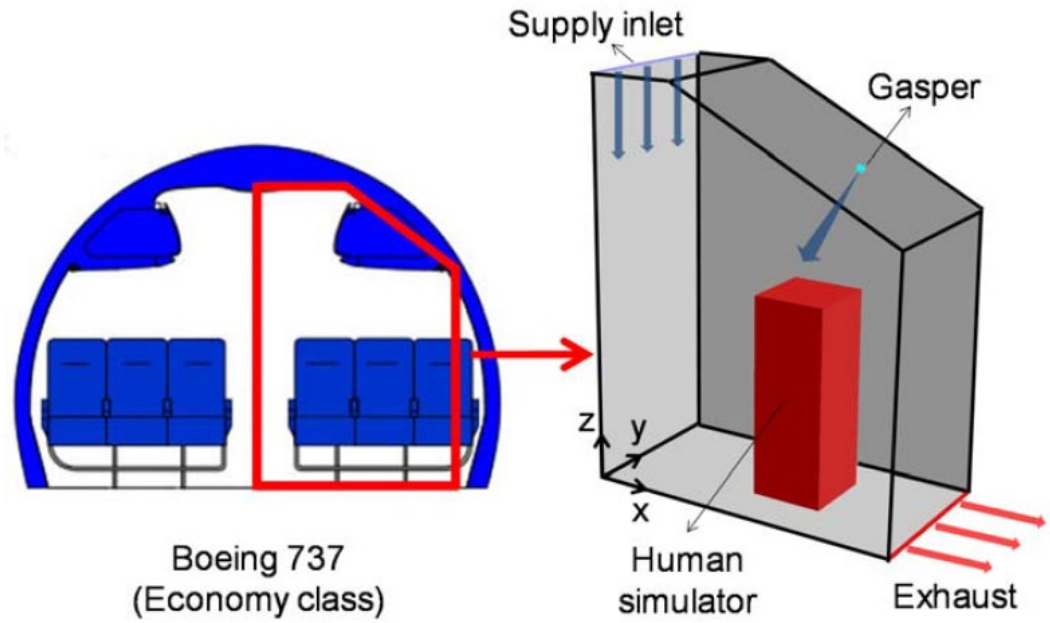

Figure 2.2-2- Boeing 737 Aircraft Cabin Mock-up by Liu et. al.'s [27]

In the literature, since the thermal comfort study for military aircraft has not been shared and is not open to public review, this study was the most convenient for performance evaluation. In addition, there are several other reasons to use this study as a test case. Firstly, all geometrical dimensions and boundary conditions have been given in this study. Therefore, it is easy to build the model without any confusion. Secondly, a human simulator has been used to simulate the thermal effects of occupants found in the cabin. Therefore, it contributes to the thesis case in terms of the thermal effect of humans.

Furthermore, gasper has been used in aircraft to provide personalized ventilation, similar to today's military aircraft. Therefore, it is advantageous to see the jet flow effect on the human simulator before the thesis case configurations. Finally, experimental and numerical modeling has been done, as shown in Figure 2.2-3, and two different turbulence models (k-ω and k-ε) have been conducted in the numerical part of the study. Therefore, it gives provision for turbulence modeling.

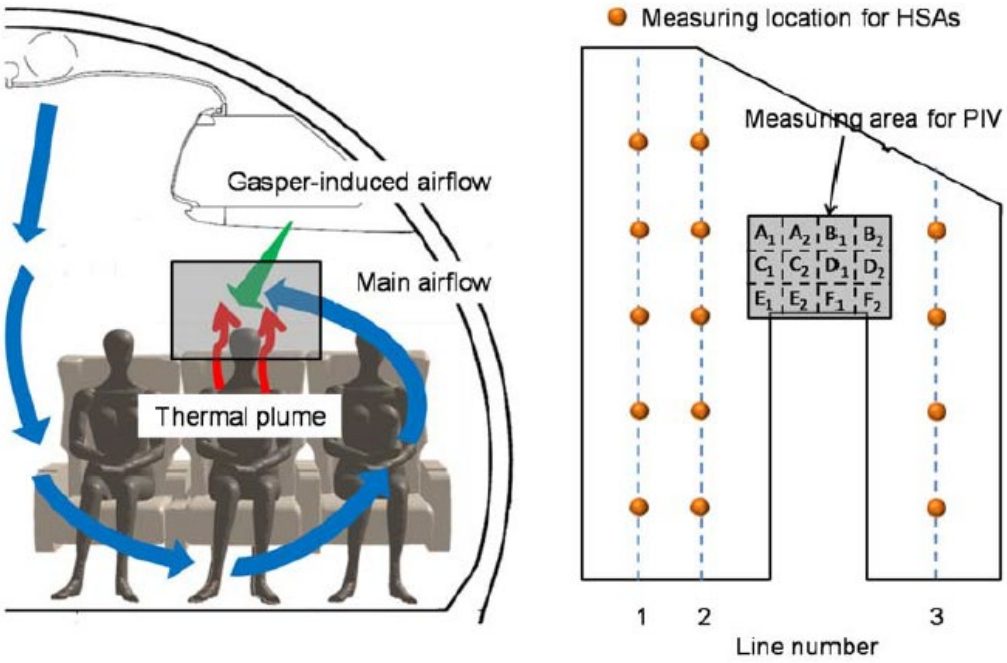

Figure 2.2-3- Experimental set-up measurement points of the study [27]

2.2.2 CFD Model Development of the Test Case

In this study, the cabin is a well-insulated enclosure. Therefore, there are stable thermal conditions. There is one occupant simulated with constant heat flux. Three symmetric wall conditions were found in the controlled volume. The left wall represents the half symmetry of the cabin, and the front & rear walls represent the other seat areas located in the front and rear of the simulated occupant. The other walls, like the ceiling, floor, and right wall, have been defined as no-slip boundaries with constant temperature distribution.

Three openings (two inlets and one outlet) are found in the controlled area. These are the main supply inlet (located at the top of the ceiling), gasper (located directly over the human), and exhaust (at the right-side wall of the floor).

The main supply inlet flows air downward with a linear diffuser, and the gasper-induced air is directed to the human. The exhaust of the cabin has zero-gauge pressure. All related detail inputs about the boundary conditions have been defined in Table 2.2.2-1.

Table 2.2.2-1- Boundary Conditions

Inputs	Values
ECS Supplied Air Velocity	1.44 m/s
Gasper Supply Air Flow Rate	1.2 l/s
Main Ventilation System Air Flow Rate	25.9 l/s
Total Air change rate	33.5 ACH (Same with Gupta et al., 2011)
Heated Human Simulator Heat Load	75 W
Main Ventilation System inlet area from velocity & flow rate	20 mm
Exhaust Gauge Pressure	0 kPag

In this study, ANSYS Fluent 19.2 has been used to develop the CFD Model. The problem is assumed as a steady and incompressible domain. Therefore, a pressure-based solver is used for the simulation. Furthermore, since the problem domain contains human heat transfer and energy flows from the boundaries, the energy model is activated during the analyses.

In the domain, the problem became complex since there is one jet-type air inlet, one linear flow inlet and outlet, wall boundaries, and human effect. Therefore, a viscous model has required to be applied. The RNG k-ε turbulence model has been chosen for the cabin air simulation to define the turbulent flow. The reason to continue with the k-ε turbulence model is the simplest, most experienced (tested), and documented model in terms of RANS models. In the literature, the RNG k-ε turbulence model is also recommended as the most appropriate model in terms of robustness and accuracy for indoor applications. [27], [29] To resolve the near-wall mesh precisely

and simulate the thermal effects in the calculation, the Enhanced Wall Treatment option was also activated in the turbulence model.

The cabin numerical model contains occupant and wall heat transfers. Therefore, the convection term is essential for the solution domain. However, the convection term tends to be nonlinear in linear momentum equations. To solve this nonlinearity, the solution requires iteration. In convection, the flow direction is crucial, and the problem becomes harder to be solved. To overcome this difficulty, a second-order scheme is used for pressure discretization, and a second-order upwinding is used for momentum and all other variables.

Continuity and Momentum equations are coupled to solve the problem. The algorithm is adopted for the coupling of pressure and velocity. The coupled algorithm has been chosen to solve the problem domain since it converges faster than the segregated solutions. However, coupled solutions require high memory requirements, but it has been preferred since there is available computer capacity for this study [26].

2.2.3 CFD Solution of the Test Case

In iterative calculations, residuals are the primary factors for convergence. It measures the error of the solution. With the decreasing residual value, the solution gives more accurate results. However, it does not mean that the solution becomes more accurate by only lowering the residual values. There are several effects available to be sure about the solution's accuracy. Therefore, three primary tools are defined in this thesis to judge the convergency.

In this thesis statement, firstly, the residual convergences have been checked. The continuity, momentum (x, y, z), energy, k (turbulence kinetic energy per unit mass), and ε (rate of viscous dissipation) equation solutions have been monitored with the iteration changes. 10^{-3} for mass and transport equations and 10^{-6} for energy equations have been targeted. The sample solution's residual results are given in Figure 2.2-4.

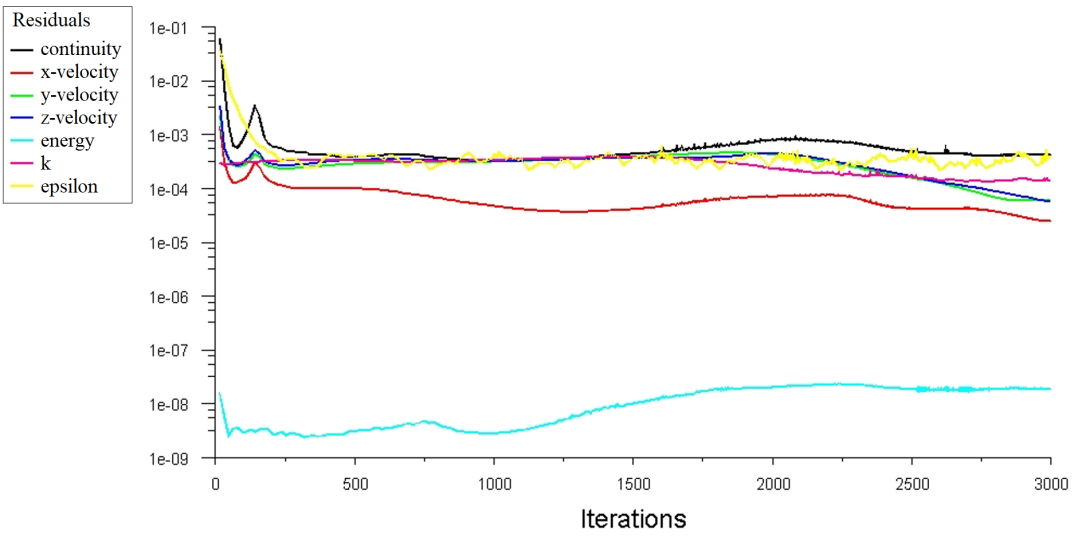

Figure 2.2-4- Residuals vs. Iteration Graph of sample solution

Secondly, the monitoring point technique has been used to ensure convergence. There are real-time monitoring points that have been defined, as shown in Figure 2.2-5. Points have been chosen to be in different locations throughout the cabin.

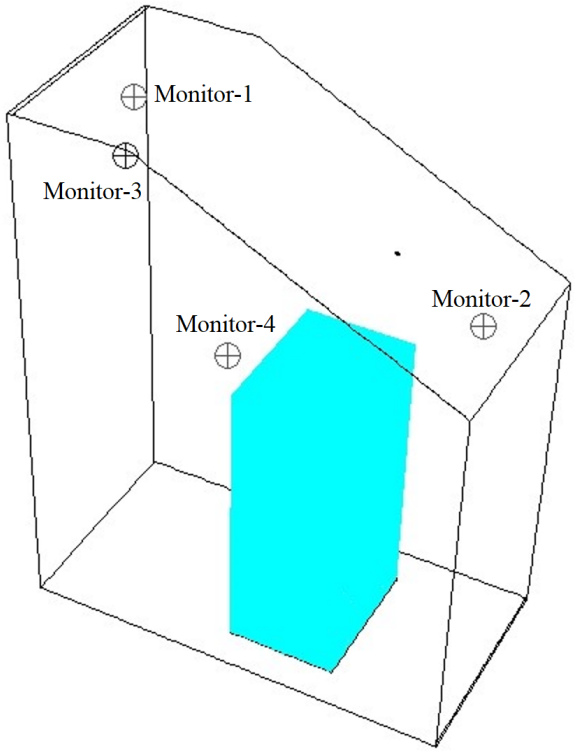

Figure 2.2-5- Monitoring Points in the cabin

The points show the variation of the calculated velocity magnitude during the simulation. The values of the velocity magnitudes converge through specific values, as shown in Figure 2.2-6. Since the simulation is steady-state, values stabilize during the simulation. All three monitoring points continued with smooth patterns except Monitor-2. However, it has also continued with a regular pattern.

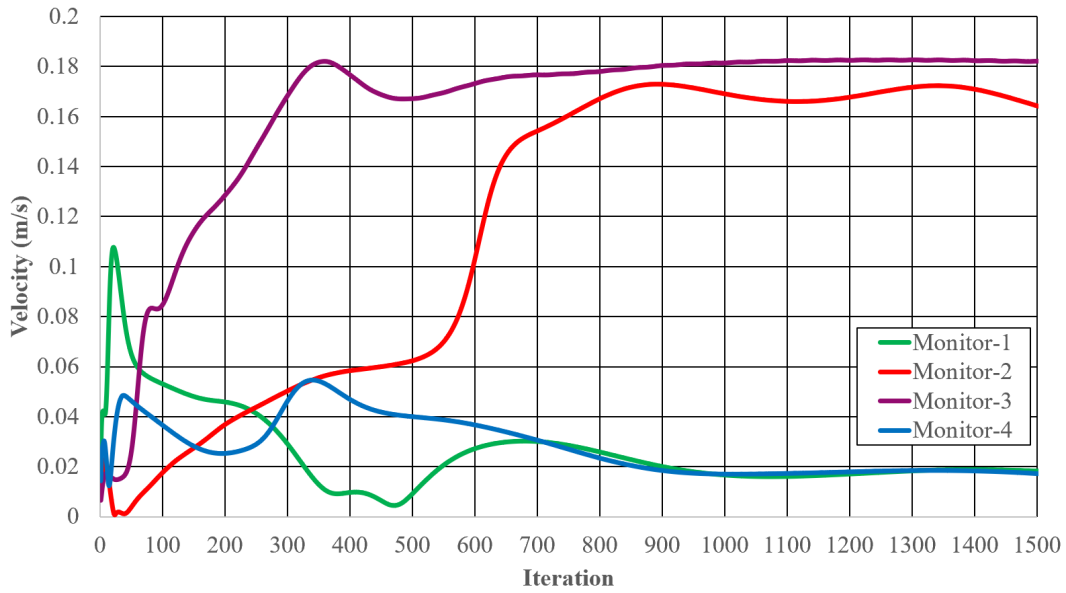

Figure 2.2-6- Velocity Magnitude (m/s) Variation graph of monitoring points during the simulation

After evaluating residuals and monitoring points, the solution's convergence has almost been sure. However, even if these two methods are applied, both provide mathematical accuracy to the equations. Therefore, a flow pattern check has also been done for the solutions of each case since a flow pattern check provides the practical meaning of the simulation applied to a physical environment. A section taken at the middle of the cabin to check the flow pattern to see the whole occupant, main inlet, gasper inlet, and outlet, as seen in Figure 2.2-7. With all three tools (residuals, monitoring point, and flow pattern) having been considered, solution convergence has been found logical and reliable.

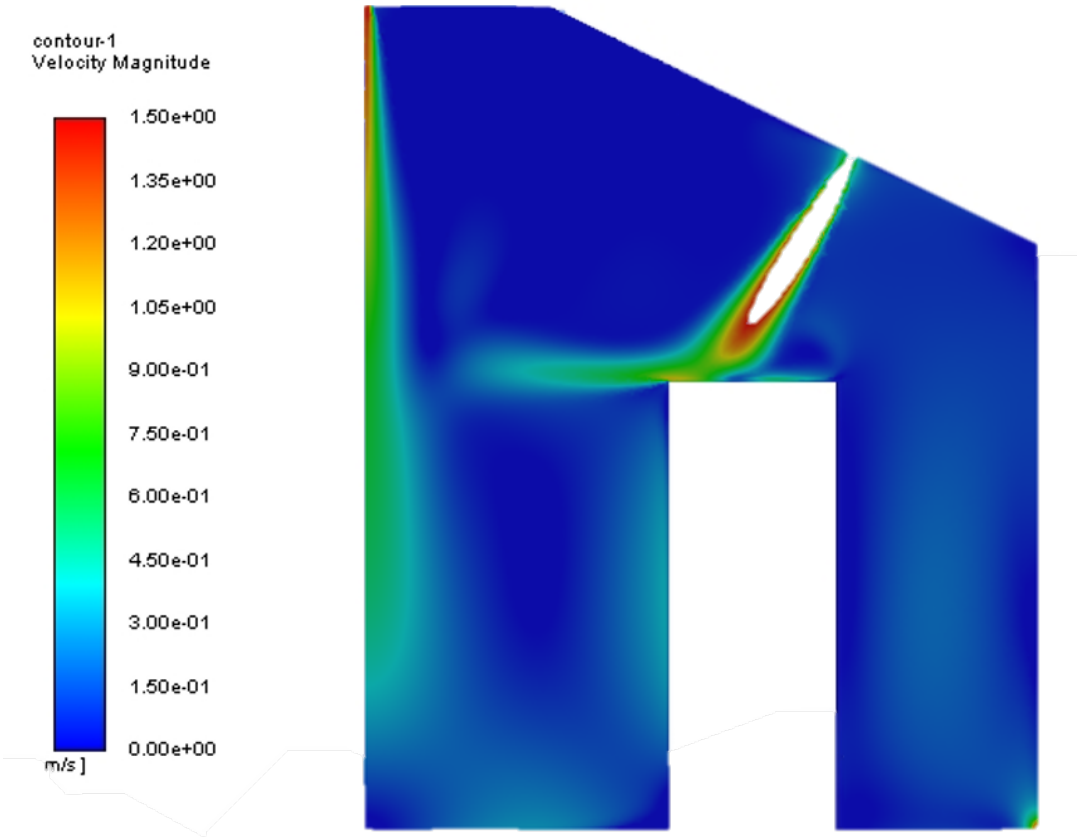

Figure 2.2-7- Velocity Contour of the Cabin for sample simulation

2.2.4 Mesh Independence Study

After being sure that the solution is converged based on the techniques defined in Section 2.2.3, it should also be required to be sure about the independency of the meshes from the solution to evaluate the performance of the chosen turbulence model.

A mesh generation study has been done over the cabin geometry defined before to evaluate the cases. Because of the complex shape of the gasper, two study have been done in terms of mesh type. Firstly, tetrahedral meshing has been applied to the cabin. Then, to keep the mesh quality at a certain standard level and catch the rapid

changes near the boundaries, an inflation layer has been applied near the wall parts (where the no-slip boundary condition is applicable) of the cabin. Smaller meshes have been used where rapid changes occur. The sample mesh of the study is given in Figure 2.2-8.

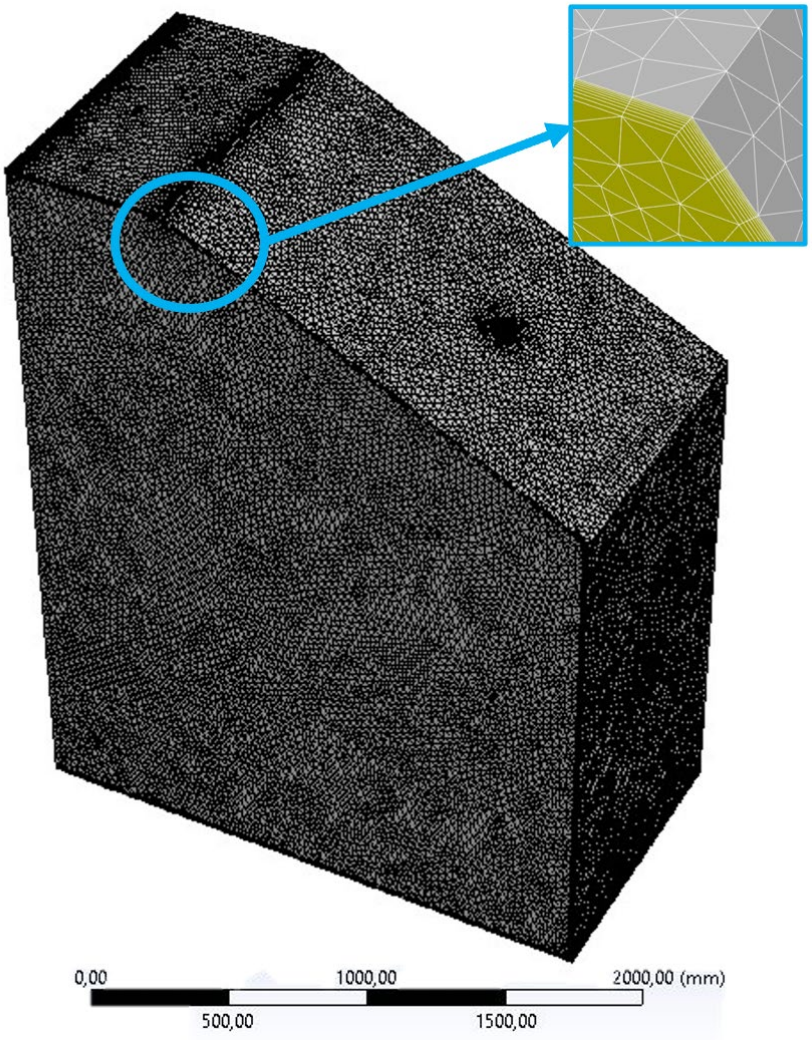

Figure 2.2-8- Tetrahedral Meshing of Sample Case

Before analyzing each mesh, mesh quality has been checked. Since with the increasing mesh quality, the solution gives more accurate results and converges fastly.

Two main measurement parameters have been used to keep the mesh quality at a certain level. Firstly, the skewness is defined for each meshing. Since high skewed cells are not appropriate for accuracy, the maximum skewness of the meshes has been tried to be kept below 0.9. As a general rule of thumb given in CFD guides, for tetrahedral meshes, this value should be kept under 0.95, and average skewness should be less than 0.33 is convenient for the mesh quality. [26]

The second mesh quality measurement defined for this study is orthogonality. The better the mesh quality, the orthogonality of the grid becomes closer to 1. [26] In the literature, this value is scaled as given in Figure 2.2-9. [30]

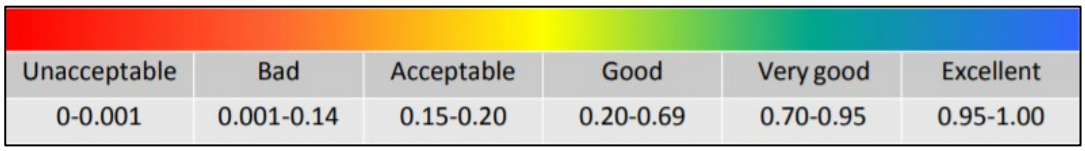

Figure 2.2-9- Mesh Orthogonality Spectrum [30]

Therefore, the minimum orthogonality value of 0.15 is aimed to keep the mesh at a certain quality. With all these parameters, mesh quality has been held at acceptable values to apply mesh independence study. The number of meshes and quality parameters are given in Table 2.2.4-1.

Table 2.2.4-1- Mesh Quality Parameters for Mesh Independence Study

	Mesh 1	**Mesh 2**	**Mesh 3**	**Mesh 4**	**Mesh 5**
Total Number of Elements	1.6 Million	2 Million	2.3 Million	3 Million	6.5 Million
Average Skewness	0.236	0.238	0.226	0.238	0.209
Max. Skewness	0.848	0.848	0.846	0.848	0.893
Average Orthogonality	0.763	0.761	0.773	0.761	0.789
Min. Orthogonality	0.152	0.152	0.154	0.152	0.150

After being sure about the mesh quality, a mesh independence study was performed. Five different mesh generations have been done. At the beginning of the study, three other parameters were defined to control and generate the mesh independence study: global sizing, regional mesh divisions, and inflation mesh sizes. During the studies, changing only the global sizing and keeping the other two parameters at certain sufficient qualities made the analysis easier, caused less computational requirement,

and found enough to evaluate the mesh independence study. Therefore, only the global sizing of the meshes has been changed, as given in Table 2.2.4-2. However, the inflation layer and near-wall treatment have been studied precisely in terms of accuracy. Since the flow rapidly changes at the near-wall regions, it affects solution accuracy. This viscous sub-layer is essential for resolving domains. In addition, for unstructured grids, since the meshes are not thin enough to capture the wall boundary layer, the CFD model requires an inflation layer to solve this region.

First, the near-wall mesh generation has been studied to obtain finer meshes at the vicious dominant regions to continue the analysis. For this study, an inflation layer has been created. Since the number of inflation layers has been affected by domain extensions, a y plus parameter is defined in the literature to resolve the rapidly changing regions. Y+ is a non-dimensional distance between the wall and the first grid node. This parameter should be in the boundary layer to detect the changes precisely. If it is not in the range, the model can be miscalculated. Therefore, the y+ value has been checked.

In this study, an enhanced wall treatment approach, in which ANSYS Fluent provides this capability, has also been used. Since near-wall flow parameters are not varying linearly, separating the boundary layer into linear pieces does not give correct results. Instead, enhanced wall treatment solves the Boundary Layer non-linearly and resolves viscous dominant regions. Conventional wisdom in CFD studies is to keep $y+ \cong 1$ for viscous affected regions and $y+ \geq 30$ for turbulent affected regions. According to this approach, y+ values have been obtained from the coarsest mesh model, as shown in Figure 2.2-10.

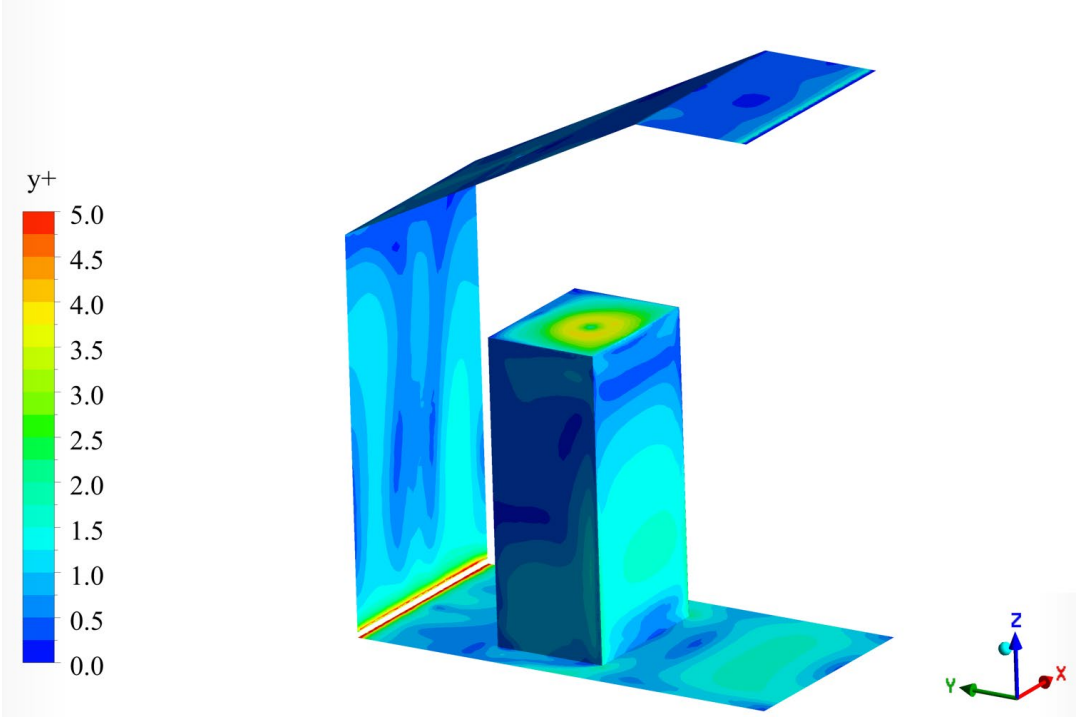

Figure 2.2-10- Sample y+ contour for coarsest mesh

The first layer thickness was kept constant in this mesh independence study. However, for the inflation layer study, the growth rate and the number of layers also affect the accuracy of the model. To solve the boundary layer correctly, the first layer thickness should have been kept less than the boundary layer thickness, and the inflation layer should have captured the boundary layer. Therefore, the boundary layer has been calculated roughly using the velocity-magnitude contour to understand how many layers are required and what the first layer thickness should be. Finally, from the default values taken from ANSYS Fluent and the general recommendation given in the literature, the growth rate has been defined as 1.2. The growth rate has not increased too much since, while the growth ratio increased, accuracy decreased because of the vast amount of changes in the volume of the meshes. Huge volume transitions are not intended since it causes gradient errors for velocity and temperature profiles [26].

After ensuring each part of the problem domain has been captured with meshes, global sizing has been changed to check the mesh independence study. At the same

time, changing the global sizing maximum inflation layer thickness has been kept in mind so as not to cause substantial volume changes and to not leave any smaller mesh sizes than the biggest inflation layer cell.

Finally, global sizing, the first layer thickness, and the number of layers has been defined in Table 2.2.4-2.

Table 2.2.4-2- Mesh Generation Parameters

		Mesh 1	Mesh 2	Mesh 3	Mesh 4	Mesh 5
Meshing	Global Sizing	30 mm	28 mm	25 mm	22 mm	16 mm
	Inlet	9 mm	9 mm	9 mm	9 mm	9 mm
	Outlet	9 mm	9 mm	9 mm	9 mm	9 mm
	Side	9 mm	9 mm	9 mm	9 mm	9 mm
	Gasper	1 mm to 0.25 mm	1 mm to 0.25 mm	1 mm to 0.25 mm	1 mm to 0.25 mm	1 mm to 0.25 mm
	Edge Sizing around the Human	5 mm	5 mm	5 mm	5 mm	5 mm
Inflation	First Layer Thickness	1 mm	1 mm	1 mm	1 mm	1 mm
	Maximum # of Layers	8	8	8	8	8
	Growth Rate	1.2	1.2	1.2	1.2	1.2
	Total Number of Elements	1.6 Million	2 Million	2.3 Million	3 Million	6.5 Million

Five different mesh studies have been carried out in the mesh independence study. The coarsest mesh has almost 1.6 million elements, and the most refined mesh has 6.5 million elements. There are two lines described in the cabin to define the mesh solutions independently, and outlet flow parameters have been checked.

Firstly, the cabin outlet flow parameters have been checked: pressure, temperature, and velocity.

According to the results given in Table 2.2.4-3, outlet flow conditions do not change with huge discrepancies. However, this is not enough to check the mesh independence. Therefore, velocity profile checks have been done for different locations defined in the cabin.

Table 2.2.4-3- Cabin Outlet Flow Conditions for different mesh generations

	Mesh 1	Mesh 2	Mesh 3	Mesh 4	Mesh 5
Number of Elements	1.6 Million	2 Million	2.3 Million	3 Million	6.5 Million
Outlet Pressure (Pa)	-2.532	-2.493	-2.479	-2.474	-2.455
Outlet Temperature (K)	294.063	294.036	294.057	294.062	294.088
Outlet Velocity (m/s)	1.903	1.905	1.905	1.902	1.892

Two lines have been defined in the test cabin. The coordinates of these lines are the same as the line described in [27]. The lines for the mesh independence study are shown in Figure 2.2-11.

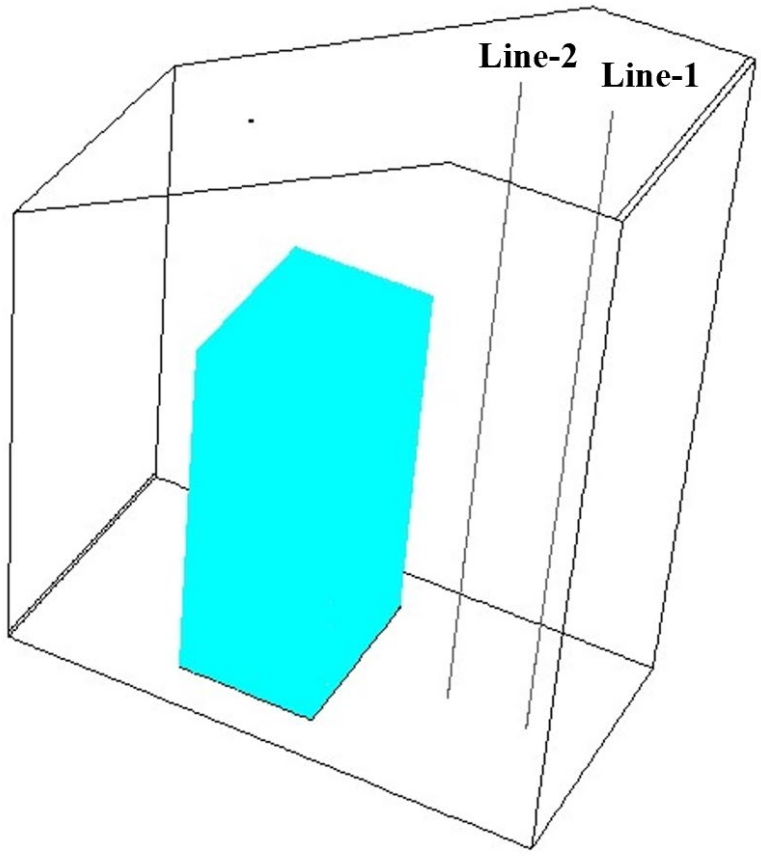

Figure 2.2-11- Mesh Independence Study Parameters

Using the lines defined in Figure 2.2-11, velocity magnitude profiles have been created, as shown in Figure 2.2-12 and Figure 2.2-13. The reason that five different meshes are used is to see the coarsest and finest mesh differences. The mesh

independence start point can be seen clearly when the mesh numbers are more than three.

When both graphs have been evaluated, after Mesh-2, results of velocity magnitude are not changing with huge differences. As a result of these figures, it can be said that meshes are independent of each other. Therefore, the best mesh should be chosen to continue the validation process of the study. From the results, Mesh-4 is the best choice for the study since the number of meshes and the convergence to the solution of this Mesh-4 are seen clearly.

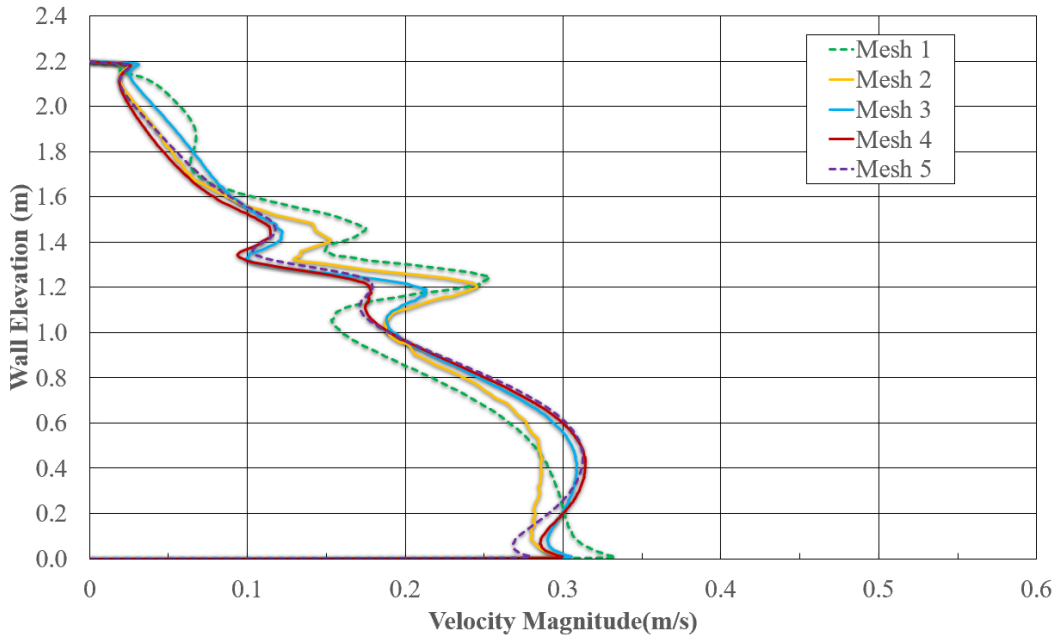

Figure 2.2-12- Mesh Independence Study Results of Line-1 (Velocity Magnitude vs. Wall Elevation)

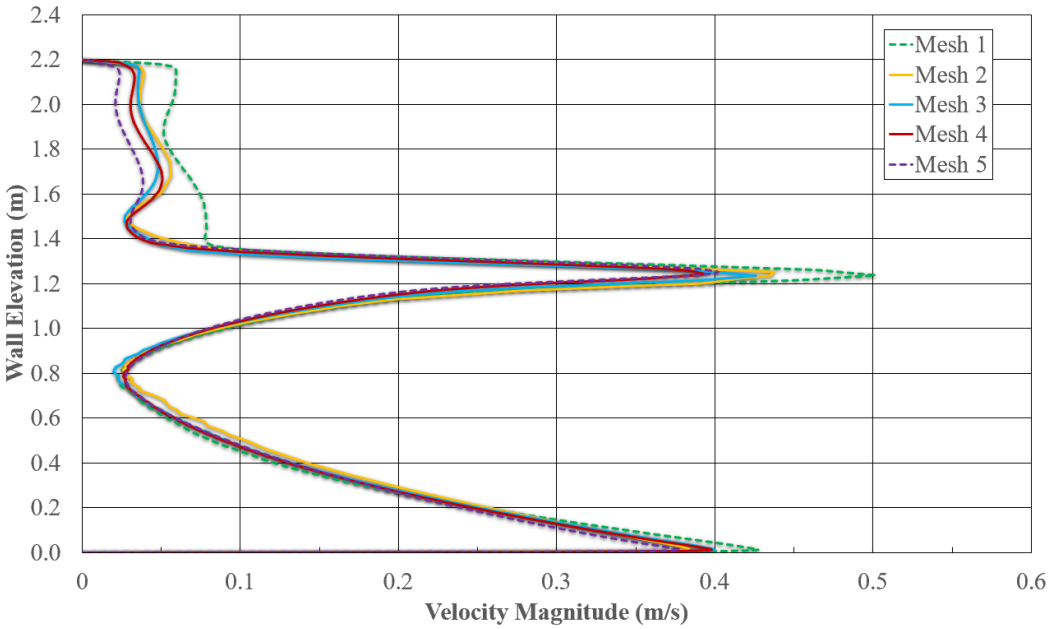

Figure 2.2-13- Mesh Independence Study Results of Line-2 (Velocity Magnitude vs. Wall Elevation)

2.2.5 Validation and Performance Evaluation Study

Up to this thesis section, convergence and mesh independence of the test case have been evaluated. Then, after being sure about the accuracy of the calculation, the performance of the model has been evaluated in this section.

The primary purpose of the article used for the test case [27] is to compare the turbulence models for air distribution evaluation in aircraft cabins. Therefore, this article has been found very useful for the performance evaluation and the validation of the turbulence model. Furthermore, it has already compared turbulence models and the experimental data.

In Liu et al., three methods have been used to evaluate the performance: experimental measurements, SST k-ω, and RNG k-ε turbulence models, as given in Figure 2.2-14.

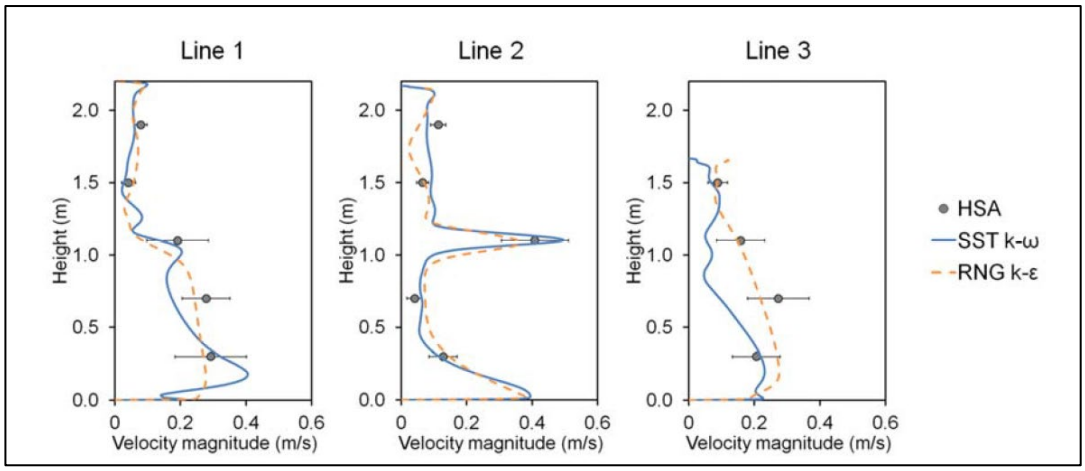

Figure 2.2-14- Comparison of the experimental and numerical velocity magnitude profiles defined in Liu et.al. [27]

To validate and evaluate the performance of the study, there are three lines defined in the article, as shown in Figure 2.2-15. In the experimental measurements, hot-wire spherical anemometers have been used to measure the velocity magnitudes throughout the lines. In addition to general cabin flow velocities, to capture the flow of the head of the occupant, Particle Image Velocimetry (PIV) has been used since the flow at the head of the occupant is complex and gasper-induced.

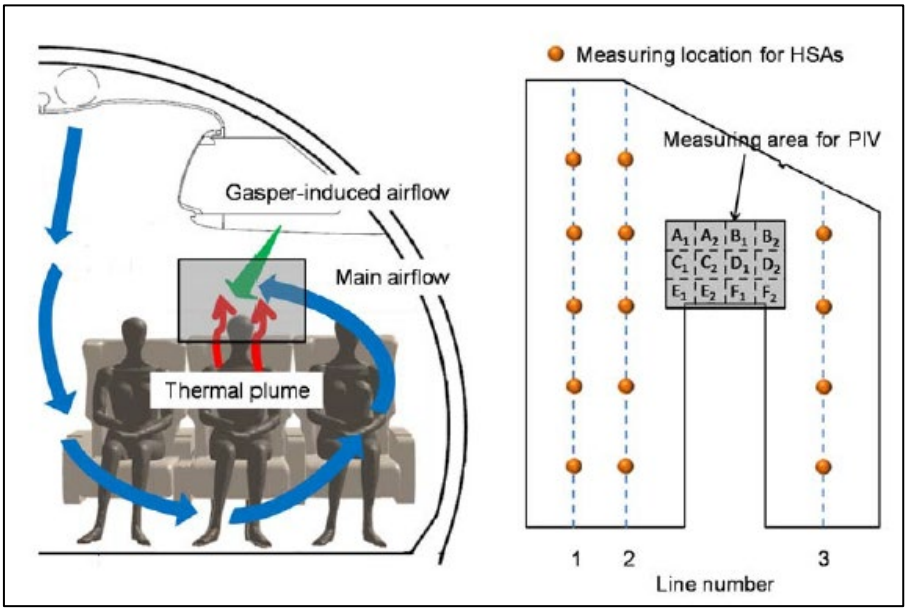

Figure 2.2-15 Measurement areas defined in Boeing 737 Cabin [27]

Two numerical methods that have been compared with the experimental study. According to the results of these studies, PIV had better resolutions in the highly flow-induced areas, but when the turbulence models were compared, k-ω had more accurate results in these areas. However, for the other main areas where the flow-induced is limited, the k-ε model gave better estimations than the k-ω model. Therefore, since the k-ε model is the most widely used tested and cheapest one, the RNG k-ε model has been considered to use in this thesis. To compare the results, Line-1 and Line-2 have been used. Totally five different meshes have been used in the mesh independence study, and Mesh-4 has been found to be the most efficient one to be used for the validation studies since there are no significant changes captured after Mesh-3.

In Line 1, when three models have been compared with the experimental data, each one seems to have different pros and cons. The current study, which uses the RNG k-ε model, has almost captured the flow in the interior part of the cabin as well as experimental data, and it gave the results in the tolerance limits. However, near the ceiling part of the cabin, a slight difference was found from the other turbulence models, but this can be underestimated according to the experimental data.

After the comparison with experimental results, the RNG k-ε model seems enough to be used in similar calculations. Standard k-ε model and k-ω models seem also useful to be used in the study, but since the RNG k-ε model captures the flow better than Standard k-ε model and cheaper and widely used for cabin comfort analysis than k-ω model, it has been chosen for the further studies. In addition, having enough computational capacity is another advantage to continuing with the RNG k-ε model.

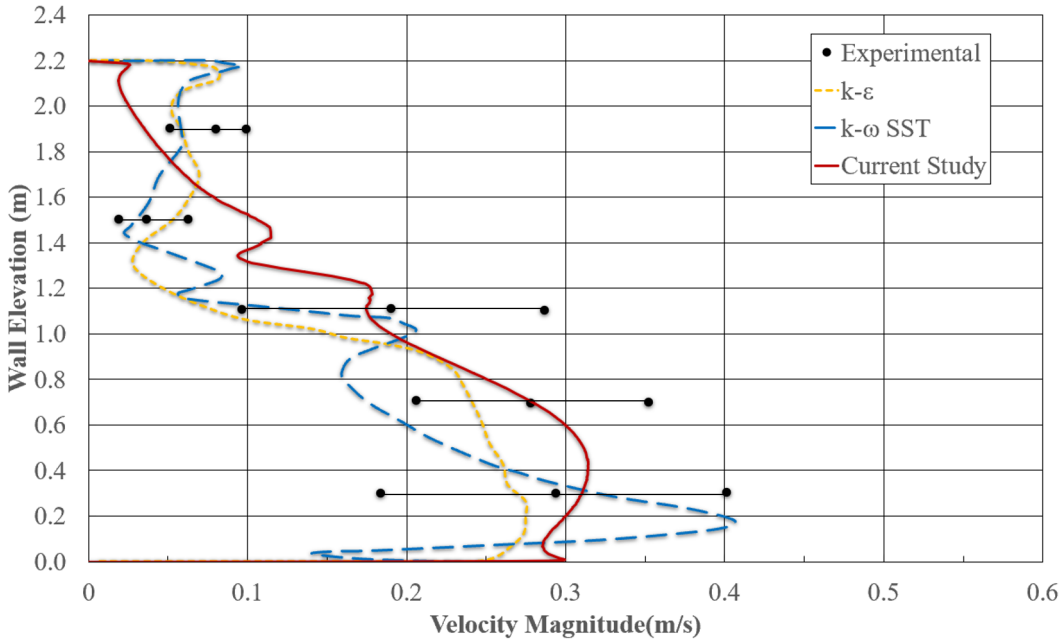

Figure 2.2-16 The Comparison of Velocity Magnitude Profile of Line-1 with Liu et al.'s. [27]

In Line 2, the flow area is closer to the human body and the effects of the flow-induced area are just at the occupant's head. The velocity magnitude lines have been drawn, and all three of the turbulence models have almost given similar and good results. RNG k-ε model that has been studied in this thesis has matched with the experimental results except the ceiling part of the cabin. At the top of the cabin part, which is a low-velocity region, a slight velocity discrepancy occurred. However, since this part of the cabin is not the interested region for the thermal comfort studies, this can be underestimated, or special refinement can be added to ceiling region, and flow can be resolved.

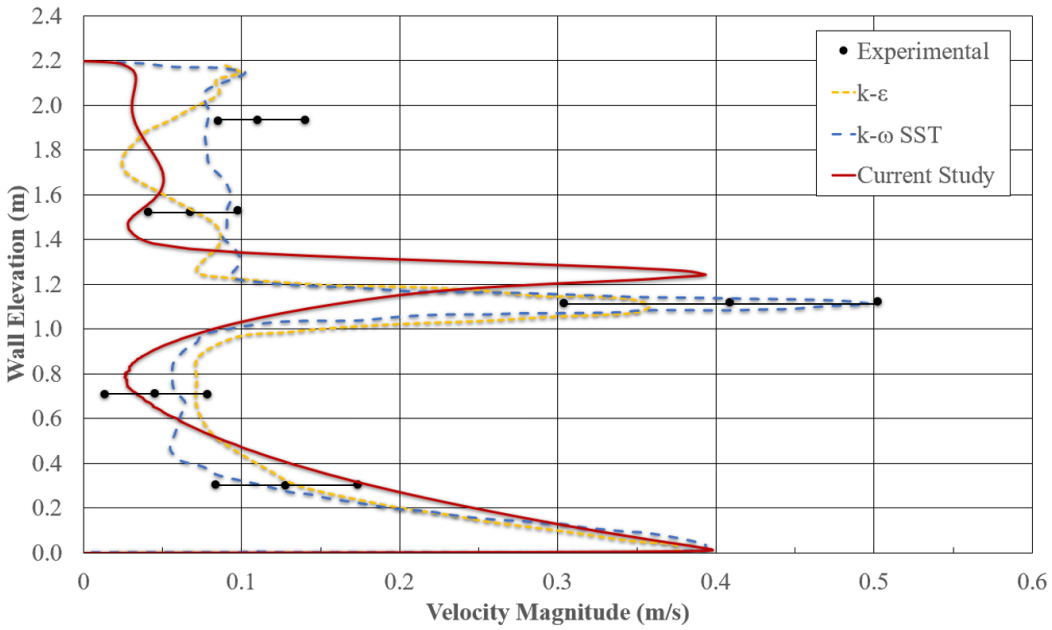

Figure 2.2-17 The Comparison of Velocity Magnitude Profile of Line-2 with Liu et al.'s. [27]

In addition to flow profile comparison, one final crosscheck with flow pattern for the turbulence model evaluation has been done. For this, there is a flow field defined over the head of the occupant which is exposed to jet flow from gasper. This region has been defined as a critical region in [27] and different resolutions of images have been taken from this area. This area has been given in Figure 2.2-15 with "measuring area for PIV". Other than the lines defined at the beginning of this section, PIV measurement technique has been used in this region since it has higher resolution capability and lower uncertainties than hot wire anemometer technique according to [27]. When the measurement taken with CFD compared with the contour defined with PIV in [27], CFD calculation gave similar flow pattern with the experimental results as given in Figure 2.2-18 and Figure 2.2-19.

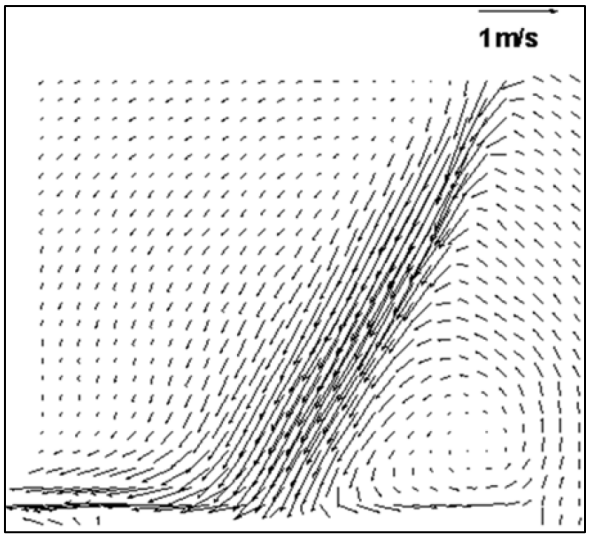

Figure 2.2-18- PIV Measurement Flow Pattern taken in [27] from the critical region of the cabin

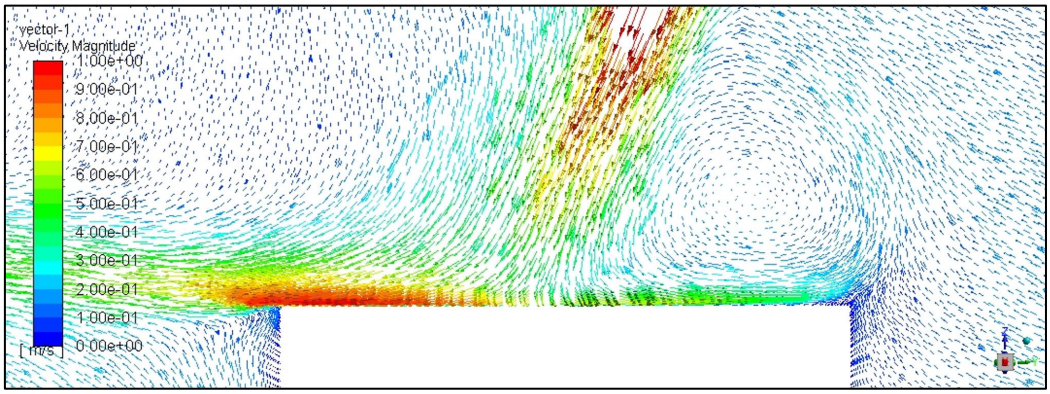

Figure 2.2-19- Velocity Contour taken from Critical Region with CFD calculations

As it is seen from these two figures, jet air is weakened after it crashes to the head of the occupant. There is a vortex structure has been formed at the right-hand side of the jet flow in both techniques. It may be caused because of the jet flow interaction with the occupant generated heat transfer. According to the results, velocity magnitude is also almost same with the PIV results. Therefore, the RNG k-ε turbulence model can be taken as sufficient for the further CFD calculations for these types of cabin flow structure analysis.

CHAPTER 3

THERMAL COMFORT ANALYSIS MODEL INVESTIGATION FOR MILITARY AIRCRAFT CABIN

In this part of the thesis, typical one-seated military aircraft cabin thermal comfort model have been investigated as given in Figure 2.2-1. The flow structure around the pilot and the effects of the thermal comfort factors have been studied.

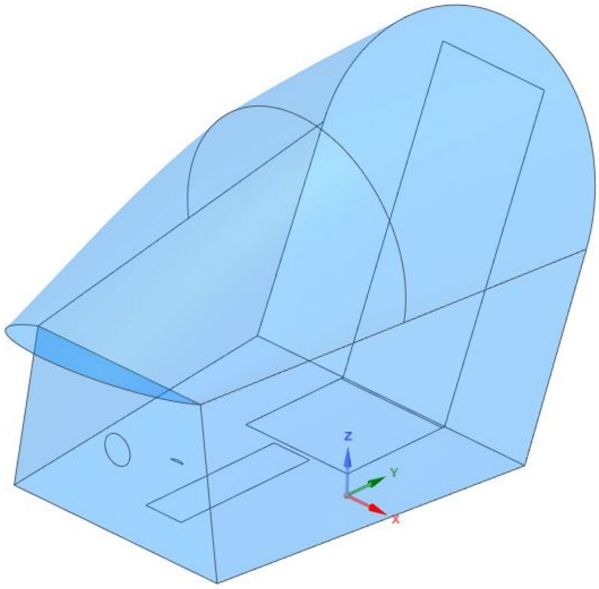

Figure 2.2-1 Sample Cockpit Model of Military Aircraft

3.1 Thesis Case: Problem Description and CFD Model

For this study, typical one-seated military aircraft model has been chosen to be evaluated. The aircraft has almost max. ceiling altitude of 50,000 ft. and 2.0 Mach max. velocity levels. When the operational cases have been investigated, since it is hard to cool down the bleed air that taken from the engine during the ground operations, ground static case for hot day condition has been chosen to evaluate the

thermal comfort of the pilot. The hot day condition has been defined according to the NATO STANAG-2895 [31] for Turkiye's climate conditions which is almost ISA+28°C. This temperature has been taken as same for every part of the ambient for the simplification. In real case, according to the position of the aircraft, there will be some shadows and temperatures at different part of the aircraft. In addition, since the ground static condition is considered for this case of analysis, there is no pressurization system required. Therefore, the pressure difference between the cockpit and outside ambient is assumed as zero.

The main observation required for this study is to measure the pilot thermal comfort. Therefore, there is an occupant modelled for the analysis. All dimensions have been defined according to the typical one-seated military cockpit and the metabolic heat load that spread from the pilot has been defined from ASHRAE Standard as given in Table 1.4.3-1. In addition to ASHRAE standard, according to the calculations defined for standard human dimensions in Equation 1.4-2, pilot heat load has been defined almost 140 W. Again, for simplification, this value has been taken as constant and spreading from each part of the human body equally, but it will be different in reality as given in Figure 3.1-1. For the future studies, heat transfer can be separated as given in Table 1.3.1-1.

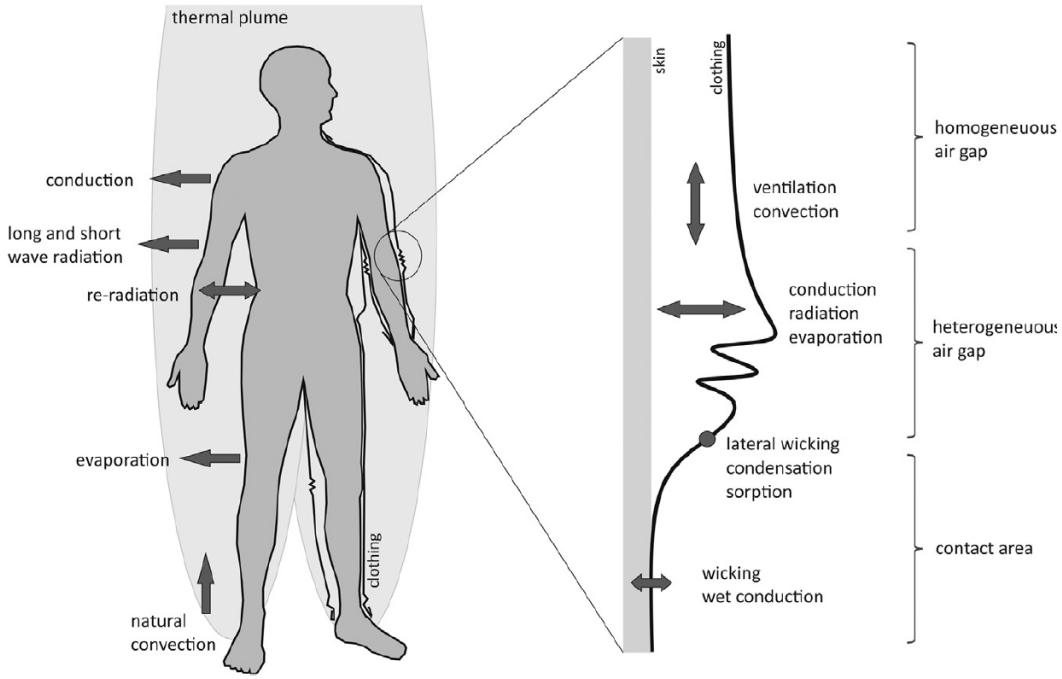

Figure 3.1-1- The tracking of heat transfer from the human to surrounding [32]

The other inputs that will gain heat load to the cockpit are defined as: solar load, cabin avionics heat loads, cabin skin & bulkhead heat loads.

Firstly, since the canopy is fully transparent, there will be huge heat transfer gain from the sun by radiation. The solar radiation for ground case is determined as 1120 W/m^2 in accordance to STANAG-2895: Table-8. From the projected area of the transparency, constant solar load enters to cabin has been assumed and calculated almost 1500 W. Although the ground case is the best condition in terms of solar radiation, the static ground case has been chosen for the analysis since the ram air required to cool down the bleed air is a harsh condition to define from the system perspective as it is mentioned before. In addition, in real life, this value can change according to the position of the aircraft. Therefore, projected area is taken according to the ground position of the aircraft.

The second heat gain will be from the structure and the skin of the cockpit. Since there are avionics bay and aircraft ambient are found around the cockpit, there will

be some heat gains through the cockpit. Cockpit has been assumed to be well-insulated and related heat transfer from these areas are almost calculated as 1500 W.

The final heat transfer to the cockpit environment will come from the avionics and the electronic equipment installed interior of the cockpit. With the developing technology, electronic equipment power consumptions are increasing. Therefore, the cooling required to cool down these equipment will also increasing. According to these observations, the heat load from the equipment have been assumed as 1000 W. It can change according to the usage of the equipment but in this case, it has been taken as constant.

In this study, different configuration of inlets and outlets have been studied to understand the best configuration for the cooling of the cockpit which will be defined in Section 4. To cool down the cockpit, constant 4°C and ~0.2 kg/s air have been provided from the ECS of the aircraft from the inlets of the cockpit. This temperature can increase or decrease according to the insulation applied over the ducts and the surrounding temperature in real aircraft. Therefore, well-insulation assumption over the ducting have been taken for the temperature increase from the condenser to the duct outlet of cockpit.

All inputs that have been determined up to now has been given in Table 3.1-1.

Table 3.1-1-Input Parameters of One-Seated Military Cockpit*

Input Parameter	**Value**
Solar Load (W)	~ 1500
Pilot Metabolic Load (W)	140
Pilot Clothing (clo)	2.2 (for summer conditions)
Cabin Avionics Heat Load (W)	~1000
Inlet Air Temperature (°C)	4
Inlet Mass Flow Rate (kg/s)	~ 0.2
Outlet Conditions	Not pressurized (ΔP=0), ground conditions
Cabin Skin & Bulkhead Loads (W)	~ 1500 (well insulated)

* *The heat transfers defined for each surface have been assumed to be constant.*

In this study, one manned military aircraft cockpit has been modelled. To prevent the high computational power consumption, most of the electronic equipment, bulkhead walls and pilot model have been simplified. Pilot has been taken in static seated position in the analysis, but in real time pilots lose energy from these movements. Therefore, this mitigation has been given with the metabolic energy loss defined before. The final geometry of the cockpit and pilot have been given in Figure 3.3-1 and Figure 3.1-2.

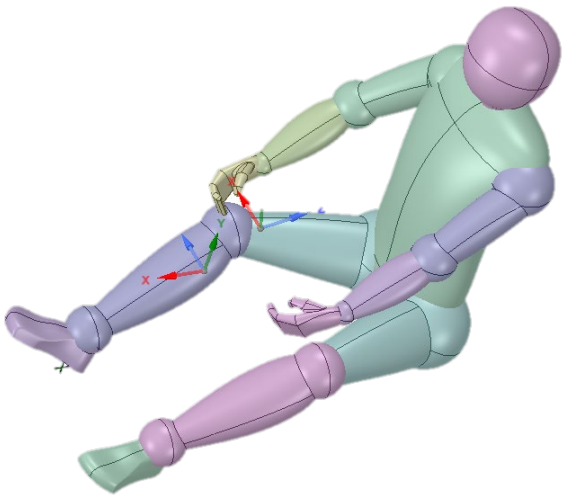

Figure 3.1-2- Simplified pilot model

3.2 Thesis case: Mesh Independence Study

In mesh independence study, piccolo type inlet configuration has been used as given in Figure 3.3-1, but the study has been done for both configuration of the cockpit. Since the piccolo configuration has more complex shape, only the mesh independence results of it have been given in this thesis. There are 16 inlets have been created for the piccolo case and the air has been assumed to exit the surface vertical of the inlets. There are four main ducting inlets have been defined for this case. Two of these ducting has been given from the back side of the pilot and the other two have been given at the sides of the pilot. Back inlets have been used for

the ventilation of the upper section of the cockpit and side inlets have been used for the lower section. For this case, outlet is given at the back side of the cockpit.

Before, evaluating the mesh independence procedure, the accuracy of the solution domain has been reviewed. To review it, four different meshes have been created firstly. 3.9 million to 12.1 million cells have been created with the help of global sizing, inflation layer and face sizing parameters as given in Table 3.2-1.

Table 3.2-1 Mesh Independence Study

	M1	**M2**	**M3**	**M4**
Cell Number (Million)	3.9 million	9.9 million	10.5 million	12.1 million
Global Sizing	200	30	25	15
Face Sizing	20	10	10	8
First Layer Thickness	2	1	0.5	0.5
Maximum # of Layers	7	10	13	13
Growth Rate	1.2	1.2	1.2	1.2

Since the geometry is complex, detailed mesh study required. Face sizing, smaller meshes and inflation layer have been applied to catch the details in the geometry where suitable areas of no-slip boundary conditions are available as given in Figure 3.2-1.

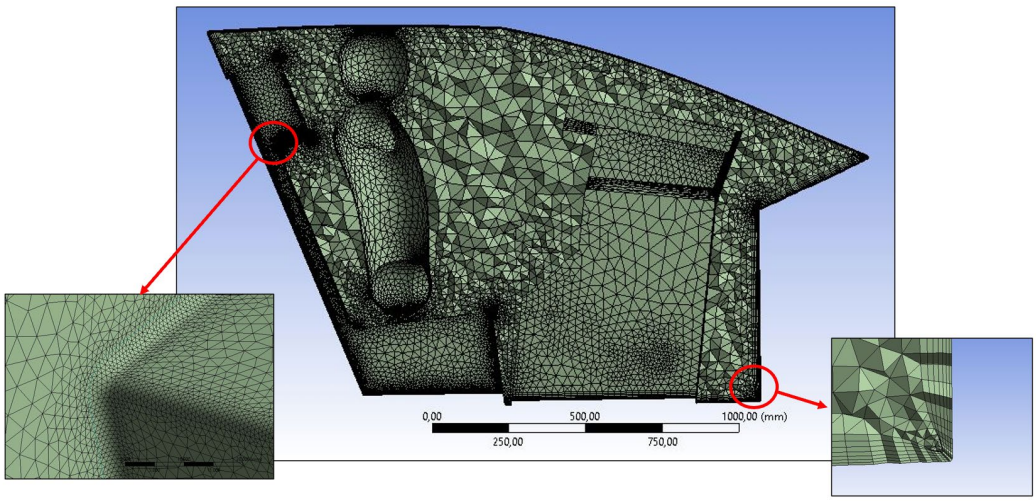

Figure 3.2-1 Sample Mesh Study for the coarsest mesh

From M1 to M4, global sizing and face sizing has been decreased. To review the mesh differences clearly, not only global size has been changed this time, but also inflation layers have been changed other than test case section. Firstly, boundary layer thickness has been calculated from the velocity magnitude contour and the minimum thickness required to capture boundary layer has been calculated. According to this input, coarse to finer inflation layer cases have been created.

Tetrahedral meshing has been used in this cockpit domain as given in Figure 3.2-1. To keep the high mesh quality, skewness and orthogonality have been defined as core parameter, but although they have been tried to be at certain quality levels, complexity of the geometry allows these parameters at some critical levels. Since there is a max. available computer source, meshes are kept at some fine limits. As a result of these studies, meshes reached to quality levels defined in Table 3.2-2.

Table 3.2-2- Quality Parameter Results of Mesh Independence Study

	M1	**M2**	**M3**	**M4**
Total Number of Elements	3.9 million	9.9 million	10.5 million	12.1 million
Maximum Skewness	0.906	0.905	0.952	0.940
Average Skewness	0.246	0.245	0.249	0.245
Minimum Orthogonality	0.094	0.045	0.048	0.059
Maximum Orthogonality	0.998	0.998	0.998	0.999

After mesh quality, residuals have been checked to ensure about the convergence of the solution of the problem domain. As a result of the residual graph given in Figure 3.2-2, the values have been seen at intended levels, but since not only the residual graph is enough be sure about the convergency, there are monitoring points defined in the cockpit given in Table 3.2-3 and Figure 3.2-3 to check the accuracy of the solution domain.

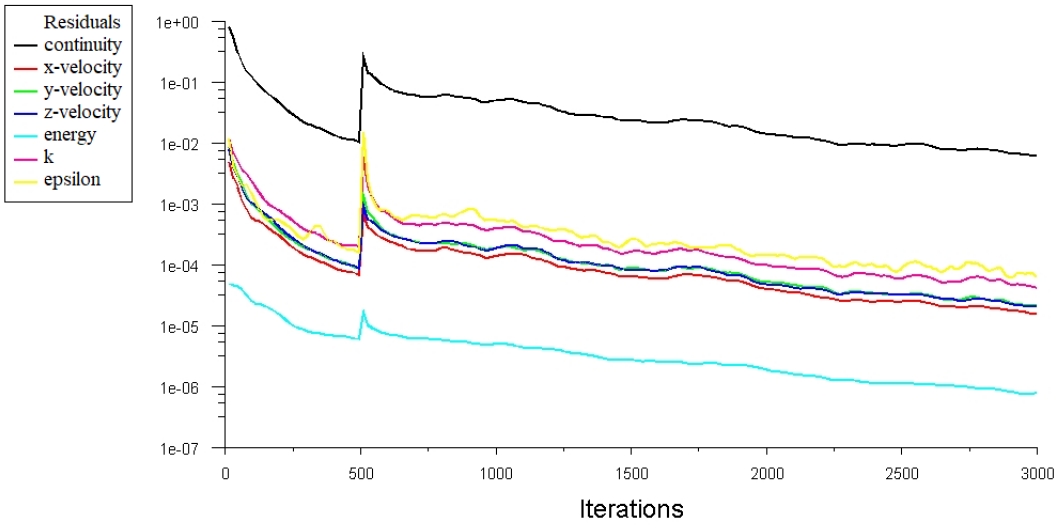

Figure 3.2-2 Residuals of Thesis Case

Table 3.2-3 Monitoring Points in Cockpit

Monitoring Point	x-coordinate	y-coordinate	z-coordinate
Point-surface monitor-1	-0.345	0.279	0.727
Point-surface monitor-2	-0.123	-0.372	0.642
Point-surface monitor-3	-0.055	-0.631	0.030
Point-surface monitor-4	-0.343	-0.014	0.621
Point-surface monitor-5	-0.342	0.400	1.000
Point-surface monitor-6	-0.342	0.279	0.400
Point-surface monitor-7	-0.342	0.350	1.100

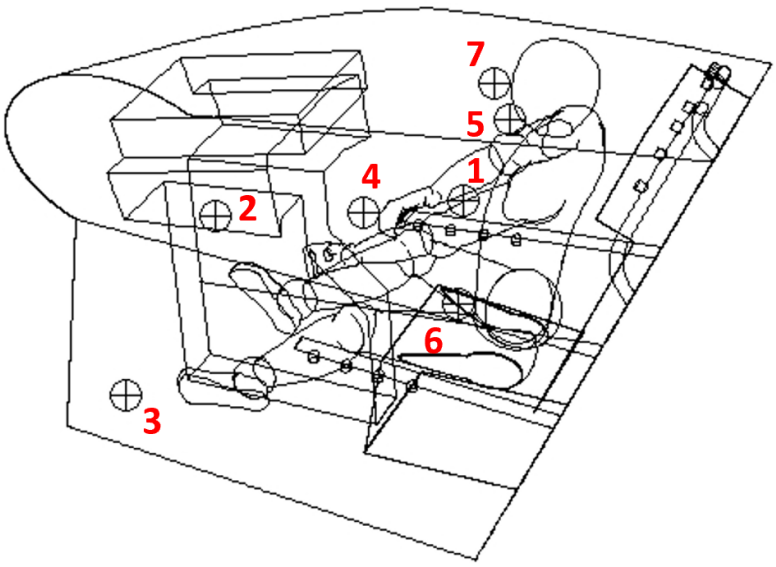

Figure 3.2-3 Monitoring Point Sketch

However, according to the results of the monitoring points, the results are converged, but they have still made some oscillations around the converged value. From this observation, it is resulted that steady solver do not stabilize when the problem domain is unsteady in some cases. Since the solver try to be in steady-state conditions for the unsteady domain. Even if the number of iterations is increased, it may not stabilize to a certain value. Therefore, for this specific problem, “pseudo-transient” property of FLUENT have been activated and the monitoring points calculated again. In conclusion, points have been converged smoother than the steady-state solver. Sample monitoring point results taken from the left and right side of the pilot (Monitor-1 and Monitor-4) have been given in Figure 3.2-4, Figure 3.2-5, Figure 3.2-6 and Figure 3.2-7.

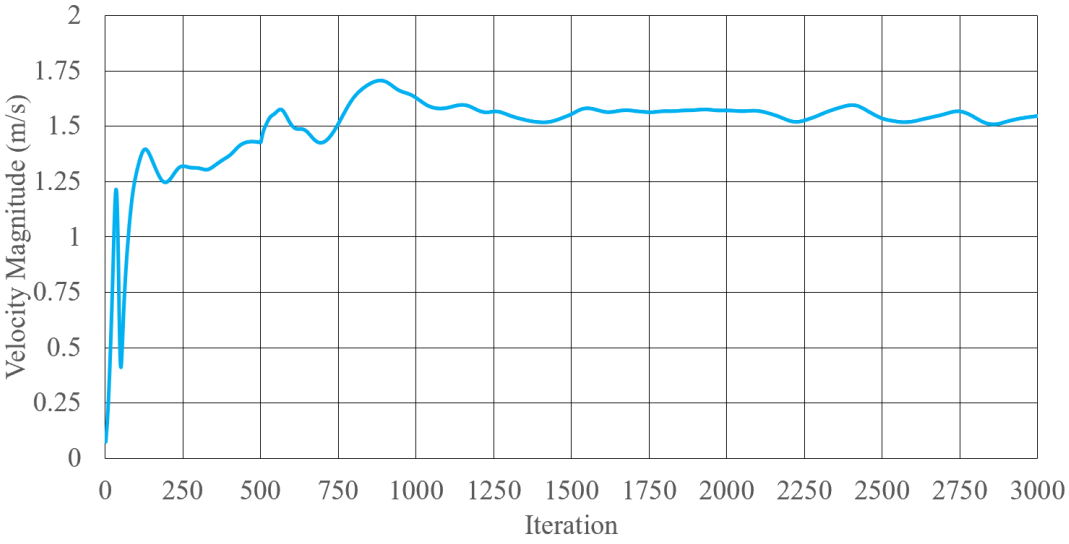

Figure 3.2-4 Monitoring Point-1 with Steady Solver

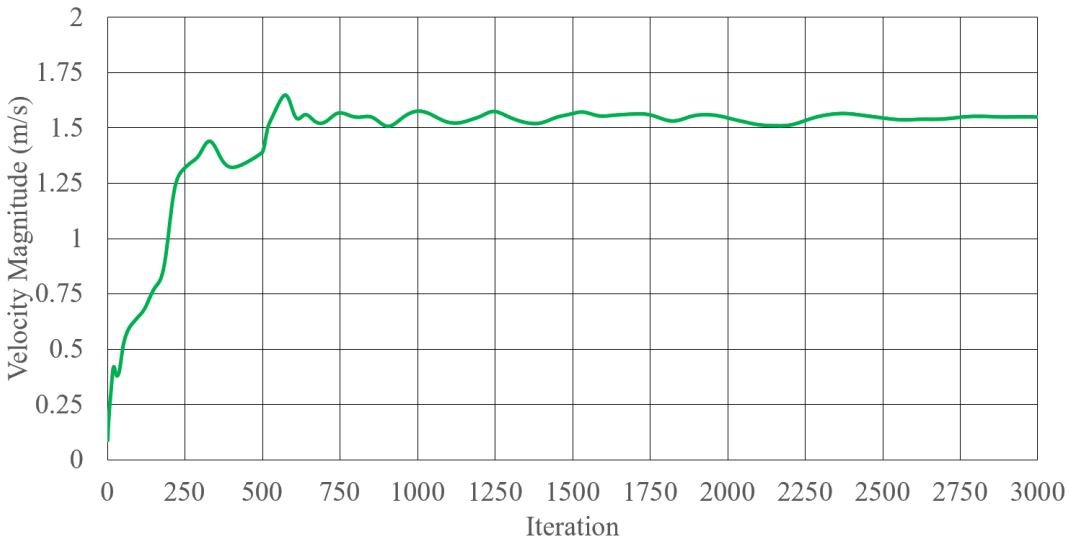

Figure 3.2-5 Monitoring Point-1 with Pseudo-Transient Solver

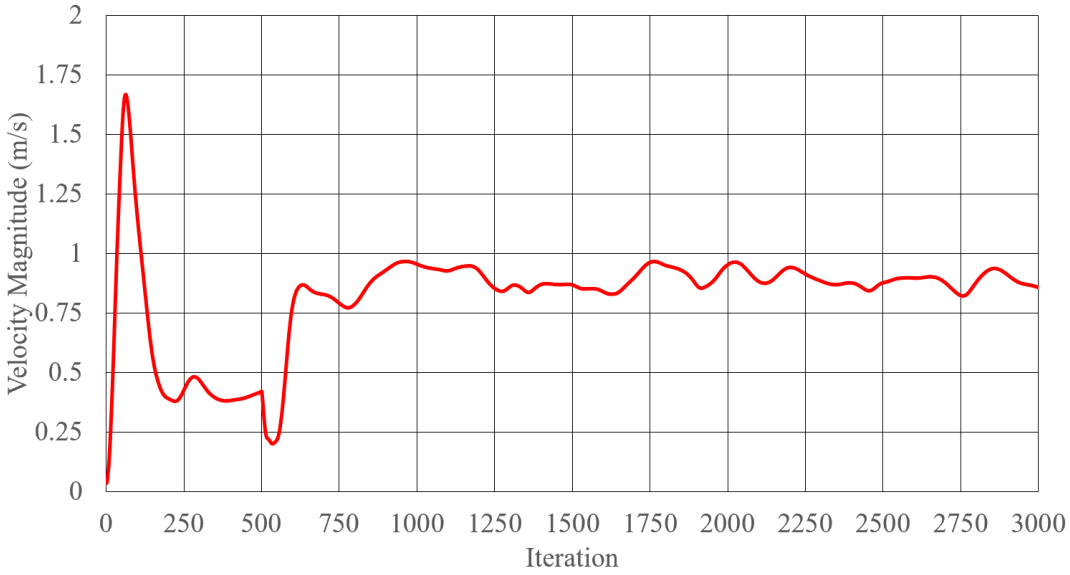

Figure 3.2-6 Monitoring Point-4 with Steady Solver

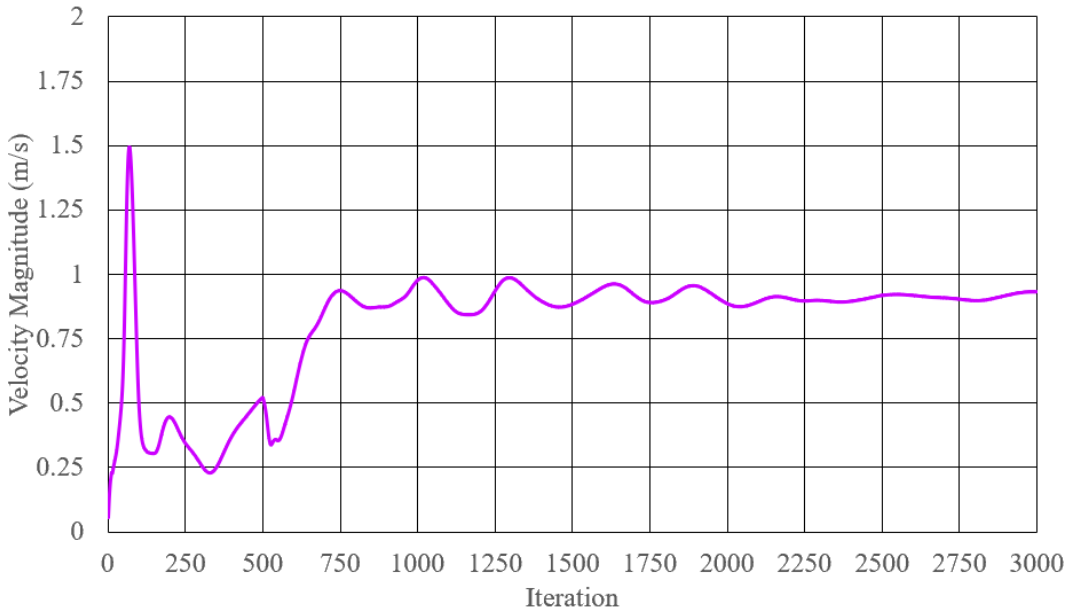

Figure 3.2-7 Monitoring Point-4 with Pseudo-Transient Solver

After convergency and accuracy check, mesh independence check is required to continue the thermal comfort study evaluations. For this issue, there are couple of lines defined in the cockpit. The line definitions have been provided in Table 3.2-4.

Table 3.2-4 Monitoring Lines for Mesh Independence Study

Lines	First Point Coordinates			Second Point Coordinates		
	x	y	z	x	y	z
Line-1	-0.34	-0.02	0.40	-0.34	-0.02	1.25
Line-2	0.00	-0.50	0.10	0.00	0.50	0.90
Line-3	-0.34	0.28	0.40	-0.34	0.35	1.10

According to the lines defined in the cockpit, velocity magnitude has been taken as the parameter that will be used in mesh independence study. Throughout the lines, coarse mesh to fine mesh comparison has been done. From the first line which is defined directly in front of the pilot, there is a convergency observed after Mesh-2.

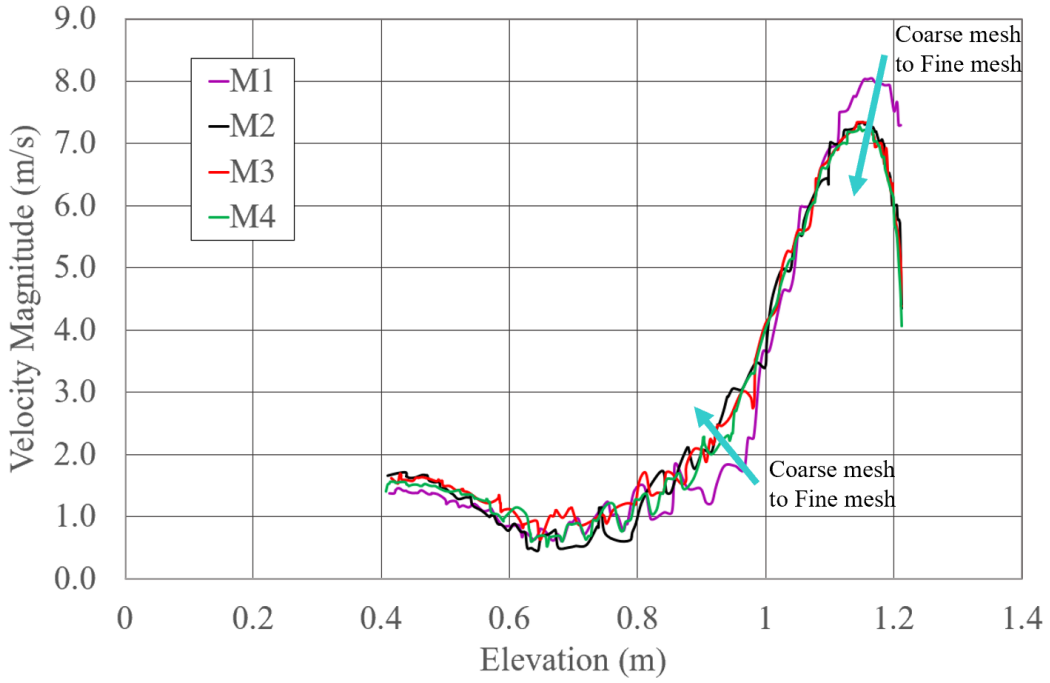

Figure 3.2-8 Velocity Magnitude - Elevation Graph for Mesh Independence Check: Line-1

As it is seen from Figure 3.2-8, velocity profiles show the same tendencies between the same velocity magnitudes. With the increase in elevation in the cockpit, velocity is increasing. To ensure the mesh independency, two more lines are also defined in the cockpit in different positions. According to the results, it can say that Mesh-4 is enough to continue the further studies. Although the same tendencies have been seen in the velocity magnitudes, again, there is an unstable environment in the cockpit, and velocities did not give smooth graphs because of the steady solver. However, this study is required to be sure about the mesh independency. Therefore, in the next step, thermal comfort evaluations will start.

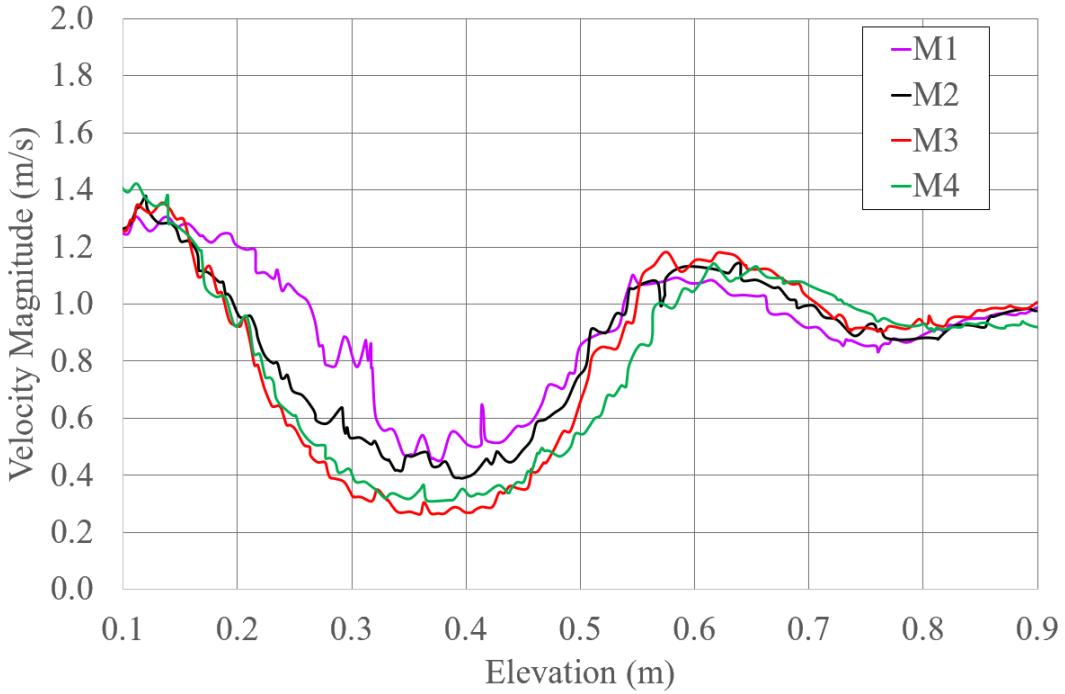

Figure 3.2-9 Velocity Magnitude - Elevation Graph for Mesh Independence Check: Line-2

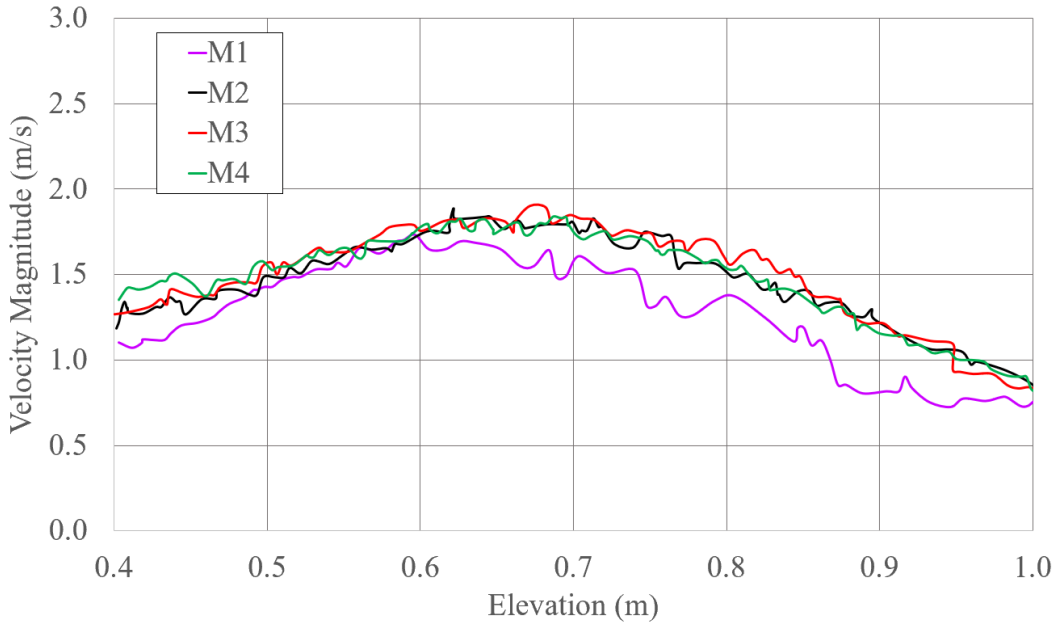

Figure 3.2-10 Velocity Magnitude - Elevation Graph for Mesh Independence Check: Line-3

3.3 Thermal Comfort Evaluation of Military Aircraft Cockpit with Piccolo Inlet Configuration

The inlet configuration effects on human thermal comfort will be evaluated in the next step, but the general approach for the evaluation of the thermal comfort with the CFD results has been discussed in this section.

As it is mentioned before, there are a couple of factors that affect thermal comfort: temperature, velocity, humidity, radiation, metabolic rate, and clothing, etc. For the evaluation of these factors, there are requirements defined in the standards which is already mentioned in Section 1.4.2. With the help of these requirements, cockpit has been evaluated as given below (according to these requirements, Mesh-4 of the analyses has been chosen to evaluate.):

From the standards defined in Section 1.4.2 requirements have been evaluated as given below:

1. **The number of inlets used in the cockpit:** as seen in Figure 3.3-1, there are more than two inlets designed for this cockpit. Almost 16 inlet exits were found to provide cooling air to the cockpit.

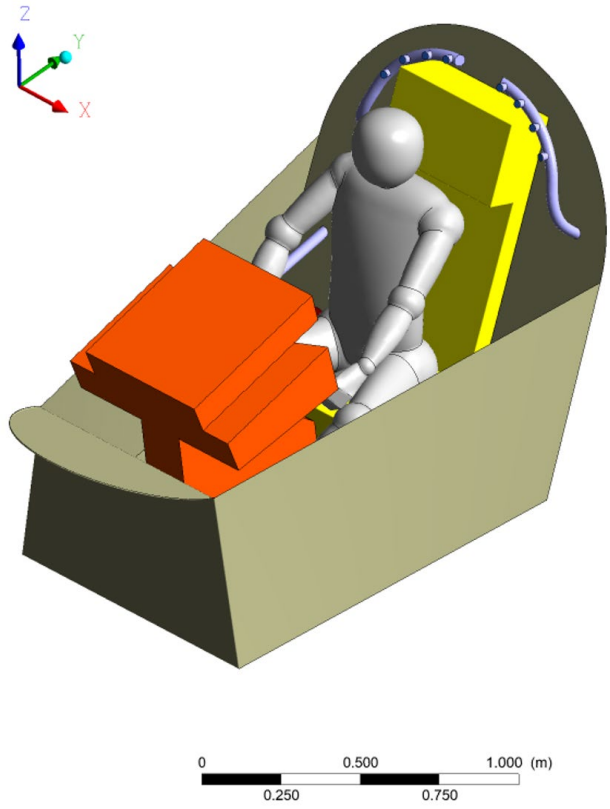

Figure 3.3-1- Geometry of Problem Domain

2. The position of the inlets: this requirement is not restricted, but it can help for the thermal comfort of the pilot. Therefore, when it is checked from the configuration, the inlets found at the back side of the head of pilot will help to cool face side of the pilot. It does not blow directly to the face of the pilot, but it can be acceptable. In addition, there are side ducting found at both side of the pilot. These channels are also used for the lateral ventilation

of the cockpit, but they are not directly blowing to pilot. Therefore, for the future analyses, its positions can be updated.

3. **Supply air temperature:** The inlet air temperature has been limited between 2°C to 71°C. When the boundary conditions have been checked, provided air to the cockpit is 4°C. Therefore, this requirement has been met with this temperature boundary condition.

4. **Temperature difference between the head and foot of the pilot:** To evaluate this requirement, temperature contour has been taken from the cockpit. There is a plane defined at the left-hand side of the pilot as given in Figure 3.3-2. At the head level, temperature is around 28°C and at the foot level, temperature is around 36°C. There is a big temperature difference with the requirement (2.8°C). Therefore, air distribution in the cabin is not at the intended levels. The left- and right-hand side cooling inlets are not enough to cool down the lower side of the cockpit.

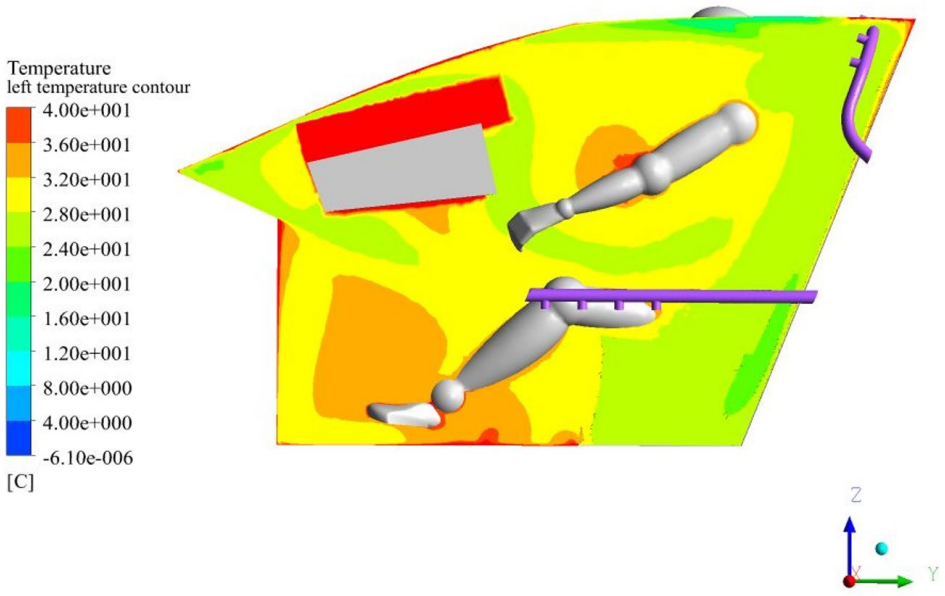

Figure 3.3-2- Temperature contour at the left-hand side of the pilot for piccolo inlet

5. Air velocity around the cockpit: Since today cockpit designs are more complex, this requirement is provided with adjustable inlets. However, this piccolo design is an old design used in the past and the inlets are not adjustable. Therefore, air is directly provided into cabin without any mass flow rate control. According to the CFD results given in Figure 3.3-3, the velocities around the pilot is higher than 1 m/s which is acceptable. At the sharp ends of the cockpit, these velocities are increasing and at the dead regions this velocities are decreasing. All in all, the velocities defined in the cockpit are seem acceptable, but for the dead areas low velocities are not enough to cool down the cockpit.

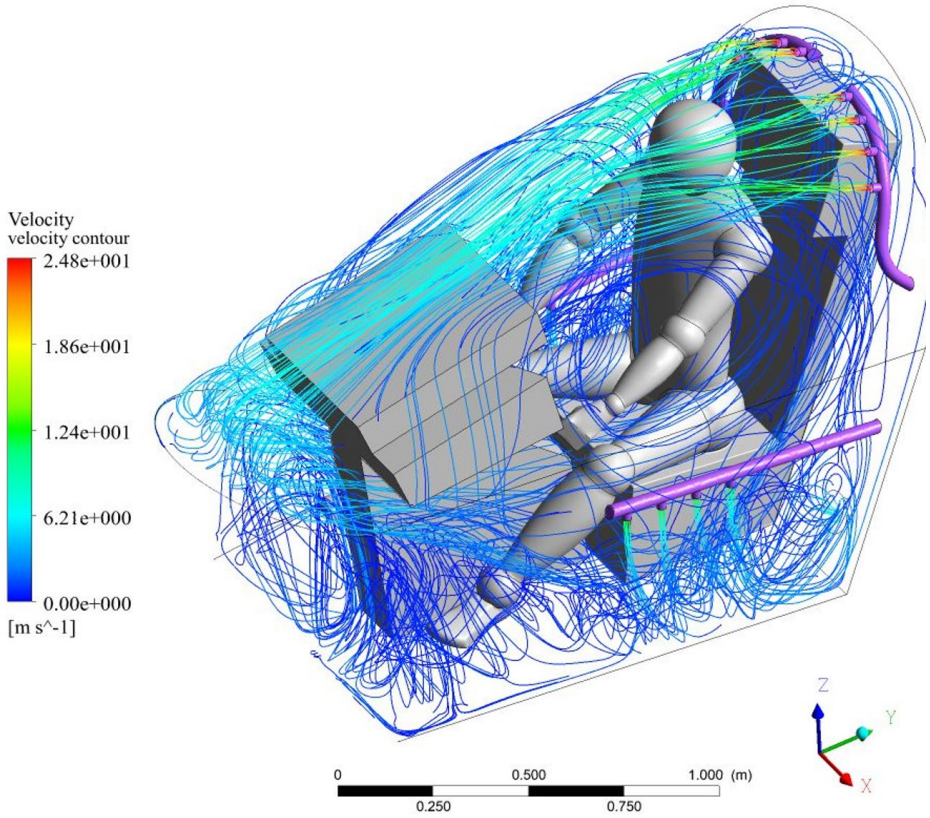

Figure 3.3-3 3D velocity magnitude streamline contour around the cockpit with piccolo inlets

6. **Exhaust Air Temperature:** According to the standards, this temperature should not exceed 35°C. When the average temperature data taken from the outlet of the model, it is around 26.69°C which is much lower than the requirement. Therefore, it can be taken as acceptable.

After all requirements have been reviewed, thermal comfort measures that defined in Section 1.4.3 are reviewed. Since the Pilot Envelope Temperature technique is the easiest way to check the thermal comfort, firstly, PET calculation has been done. According to the Equation 1.4-4, PET is calculated almost 23.29°C which is in the range of "Comfort Zone" defined in MIL-E-18927E given in Figure 3.3-4:

$$T_{out} = 26.69°C$$

$$T_{in} = 4°C$$

$$T_{PE} = 0.85 * (26.69°C) + 0.15 * (4°C) = 23.29°C$$

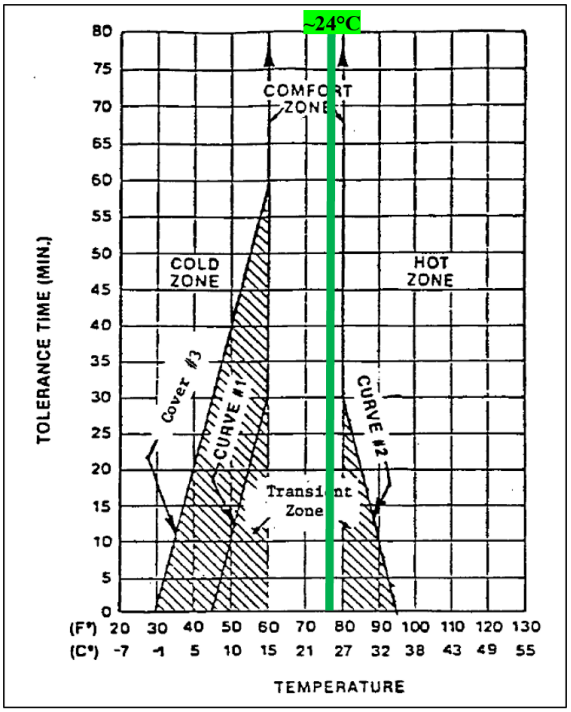

Figure 3.3-4 Thermal Comfort Check with PET [18]

Although Pilot Envelope Temperature is an easy way to understand the occupant in a comfort zone, the other techniques are also carried out since there are local hot zones in the cockpit and other factors that effect on thermal comfort.

The next step is the Wet Bulb Globe Temperature method. According to WBGT, there is a Wet Bulb Temperature and Globe Temperatures are required to investigate the method. Since the CFD results do not provide these temperatures. There are different sources used for these calculations. For Wet bulb temperature calculation, the relative humidity value has been taken from NATO STANAG-2895 for Turkiye which is %16 and average dry bulb temperature for this case has been defined as 30°C. In reality, the air provided to the cockpit is almost dry air because of the water separators used in ECS, and the only vapor source is the pilot herself/ himself. However, to be on the safe side, the worst-case scenario has been taken in this thesis. As a result, the wet bulb temperature is calculated around 14.7°C.

For globe temperature, since it is hard to defined, there is a small investigation has been done and an article is found from the literature. In this article [34], there is an estimation has been done with the meteorological data. There is an equation has been defined with these experimental results and Figure 3.3-5 provides the predicted black globe temperature related to daytime air temperature.

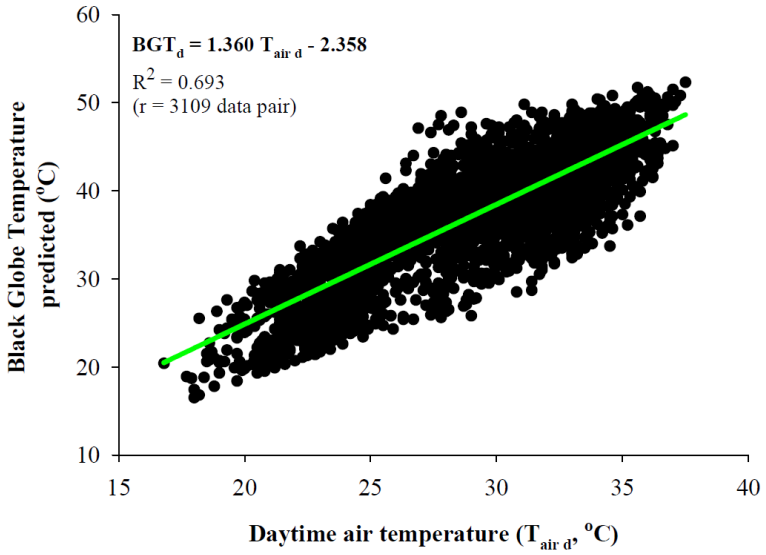

Figure 3.3-5 Predicted globe temperature correlation with daytime air temperature [34]

Correlated globe temperature with 43°C ambient temperature has been calculated as 56.1°C. It is assumed as constant. From these temperatures, WBGT is calculated with Equation 1.4-5:

$$WBGT = 0.7 * 14.7°C + 0.2 * 56.1°C + 0.1 * 30°C = 24.51°C$$

However, as it is mentioned before, clothing and metabolic rate has also effects on thermal comfort. Therefore, firstly, the total clothing insulation value 2.26 clo is inserted into Equation 1.4-3. However, when the pilot sits over the seat, then there will be an increase in insulation because of the contact area. For this, in ASHRAE 55 Standard, additional 0.15 clo is suggested to be added. Therefore, totally 2.41 clo has been used for the calculation:

$$I_{clo} = 0.835 * (2.41\ clo) + 0.161\ clo = 2.2\ clo$$

To understand the effect of clothing into WBGT, for NBC Clothing which have closer insulation value to pilot clothing [35], it is suggested to add 10°F into WBGT (°F) value in [22]. The calculated WBGT from the CFD calculations is 76.1°F (24.51°C) and when this clothing effect is inserted into this calculation, the resultant temperature is 86.1°F (30.1°C).

Finally, using Figure 1.4-5, the limits for metabolic rate is defined. The limited WBGT value for the occupant with 140 W/m^2 metabolic rate with typical 4-hour work is almost ~31°C (87.8°F). This value is defined in JSSG-2009 and MIL-E-18927E as 32°C (90°F) for ground operations. When it is compared with the resultant WBGT value, it is lower than the maximum limit. Therefore, it can be said that the average WBGT value is in the range of the thermal comfort limits. However, as it is mentioned in MIL-E-18927E, the temperature should be taken from head and shoulder. When the temperature at these parts have been calculated, at the shoulder part of the human, temperatures are at the limits. Therefore, in the next part of this thesis, different configuration of the cockpit cooling inlets will be evaluated.

Table 3.3-1 Resultant WBGT measurements from different part of the human body for piccolo inlets

	DBT (°C)	**WBT (°C)**	**GT (°C)**	**WBGT (°C)**	**WBGT (°F)**	**Resultant WBGT with clothing effect (°F)**
Head	28	13.46	56.122	23.44	74.19	84.19
Shoulder	34	17.32	56.122	26.75	80.15	90.15

CHAPTER 4

THERMAL COMFORT INVESTIGATION STUDY OF MILITARY AIRCRAFT CABIN FOR GASPER AND PICCOLO TYPE INLETS

After the model investigation and the thermal comfort evaluation has been done, different types of cabin inlet effects over the crew have been investigated in this part of thesis to evaluate the best configuration for the cooling inlets. The aircraft cockpit distribution systems are investigated from the literature, and two typical cabin inlets are decided to be used in this study.

In the early studies in time, there were piccolo type cabin inlets [36] used as given in Figure 3.3-1, and the first configuration of the cabin inlet design has been referred to this study in previous section. Using the similar method, cabin distribution system has been designed as given in Figure 3.3-2. However, there is no foot inlet defined additionally for this study. The mass flow rate has been divided into two inlets which are upper and lower ones. %33.33 of this flow rate has been directed to lower ones and %66.67 of this flow rate has been directed to upper ones. The outlet of the cockpit air is defined over the rear bulkhead.

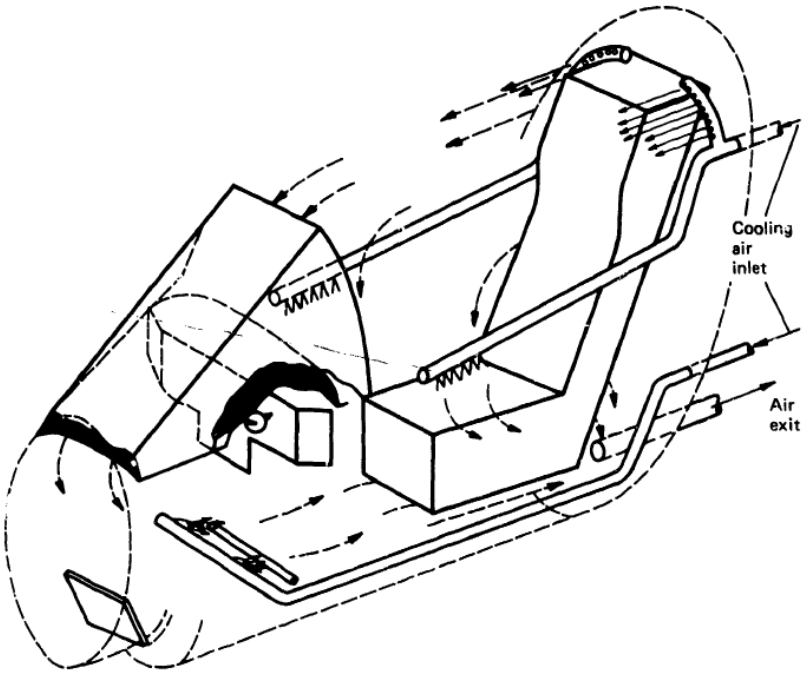

Figure 3.3-1 Cooling Inlet Configuration of TSR-2 Cabin [33]

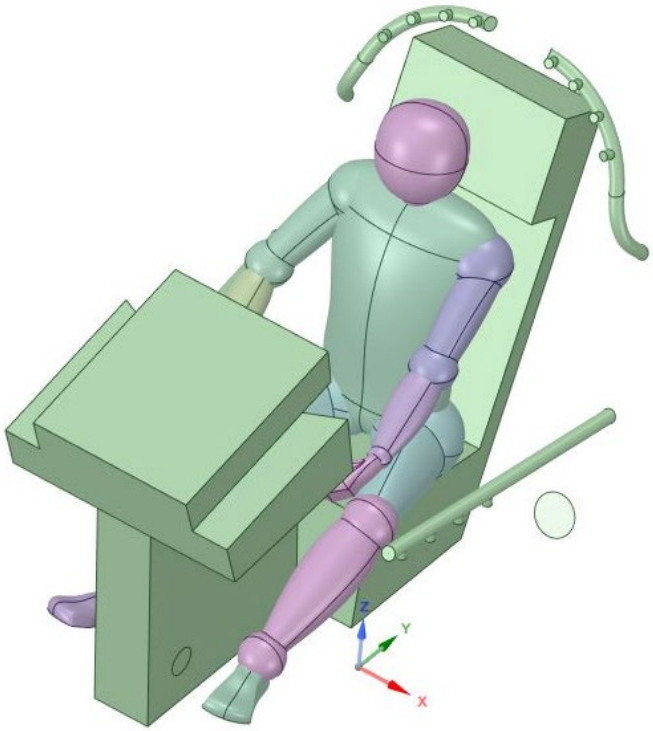

Figure 3.3-2- Piccolo Type Cockpit Distribution System for One-Seated Cabin

As time passes, inlet models have been modified, inlets have been developed, and the locations of the inlets have mostly been directed to the occupant for manual pilot control. Therefore, the second air inlet configuration has been chosen as the pilot-directed flow configuration, which refers to Figure 1.4-2 (JSSG-2009, Appendix D). Although the flow is given from the front side of the pilot, there is no rear flow inlet for this configuration, but in addition to piccolo configuration, foot inlets has been used for the cooling of lower side of the cockpit. Gasper shaped air inlet has been used for this model to evaluate the jet-flow in the cockpit and the air outlet of the cockpit has been installed over the front bulkhead. The final version of the gasper type cooling inlet has been given in Figure 3.3-3.

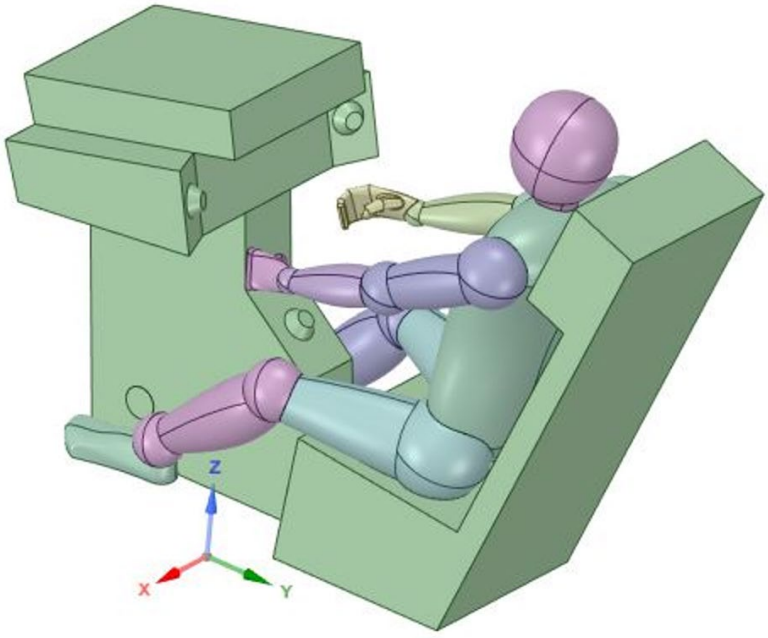

Figure 3.3-3 Gasper cooling outlet configuration

The differences between both configurations have been given in Table 2.2.5-1.

Table 2.2.5-1 Comparison of Cooling Inlet/Outlet Configurations

Cooling Outlet Configuration	Inlet		Outlet Position	Mass Flow Division
	Number of Inlets	Inlet Positions		
Piccolo	16	Rear and side	Rear Bulkhead	%33.33 Side Inlets %66.67 Rear Inlets
Gasper	5	Front	Front Bulkhead	%33.33 Foot Inlets %66.67 Gasper Inlets

After models have been created, mesh independence studies and accuracy checks have been done as given in previous section, in this part of the thesis, only the thermal comfort evaluations have been given to not duplicate the studies.

Before the detailed thermal comfort evaluation, main parameters used in Section 3.3 have been evaluated. Same inlet and outlet boundary conditions have been used in both configurations to understand the differences clearly.

There are six main parameters defined in Table 4-4. All these parameters have been evaluated for the piccolo case in Section 3.3. Therefore, each parameter is applied to the gasper case this time and both are compared according to the requirements defined in standards.

1. **The number of inlets used in the cockpit:** In gasper type inlet configuration, three main gaspers have been used as given in Figure 3.3-3, and two more inlets have been used for the lower parts of the cabin at the foot side. From these observations, gasper configuration is met the requirement. Therefore, at this criterion, both configurations provide the intended needs.

2. **The position of the inlets:** Three of the inlets are directed to the pilot's face. However, these inlets are adjustable. Therefore, pilot can change the amount of air coming to his face. In this study, inlets have not been adjusted to

compare the cases equally. However, since piccolo type partially meet this requirement, gasper case have an advantage in thermal comfort evaluations.

3. **Supply air temperature:** For the comparison of both configuration this criterion was kept same to evaluate the cases fairly.

4. **Temperature difference between the head and foot of the pilot:** In piccolo case, the difference has not been achieved as intended. However, in gasper case, the temperature difference has been measured maximum ~3°C which is very close to the suggested value given in the standard. The temperature contour defined for gasper from the left-hand side plane of the pilot is as given in Figure 3.3-4. As it is seen from the contour, there is more smooth temperature change seen throughout the cockpit in gasper configuration. In terms of temperature distribution, the lower temperature area around the pilot is more in gasper case.

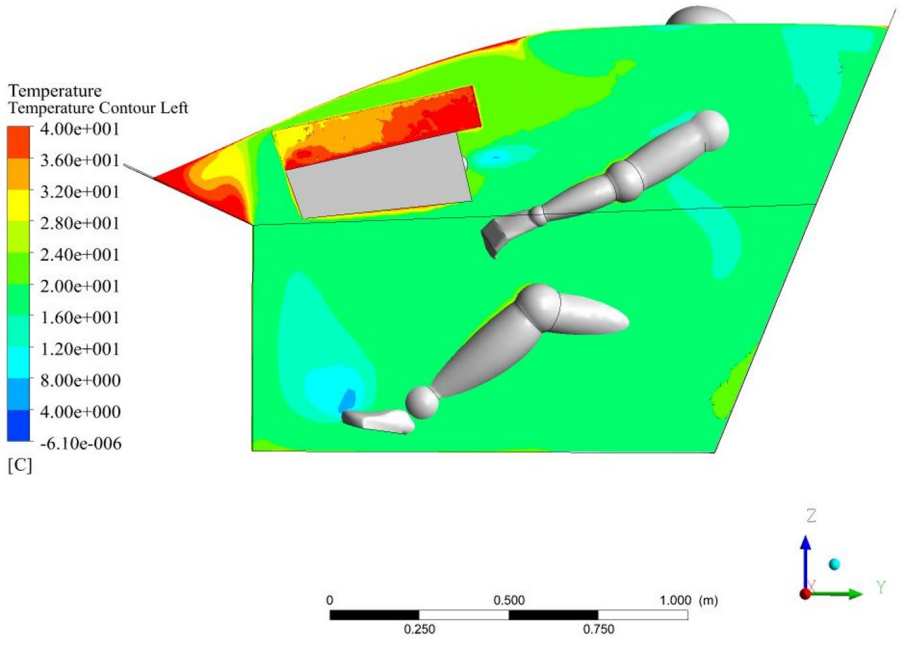

Figure 3.3-4 Temperature contour at the left-hand side of the pilot for gasper inlet

A plane is created in the middle of the cockpit to detect the temperature distribution difference between the two configurations. The configurations are given in Figure 3.3-5. From these configurations, it can be said that gasper jet flow configurations provide more effective air distribution into the cockpits.

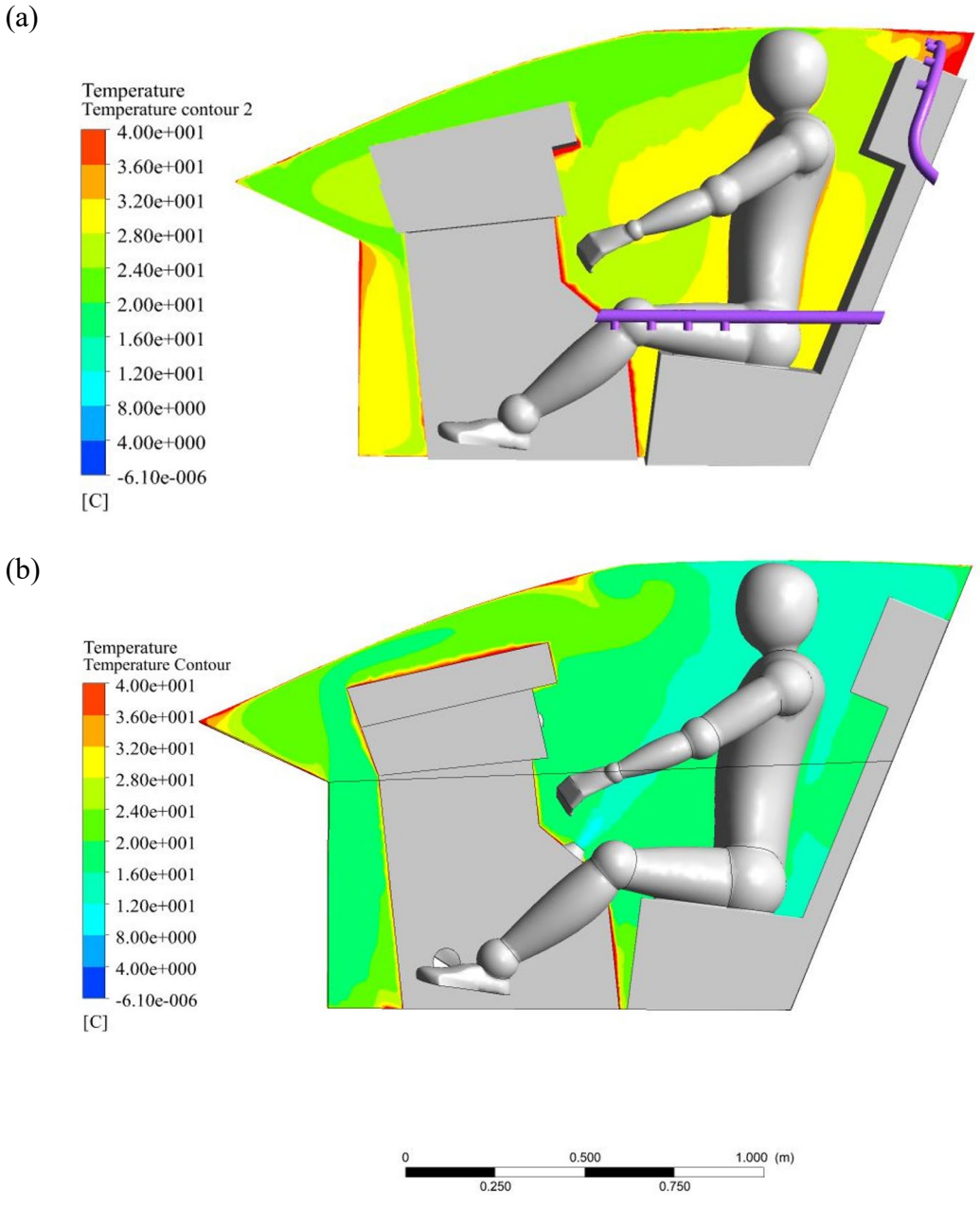

Figure 3.3-5 (a) Temperature contour of piccolo inlet (b) Temperature contour of gasper inlet from middle plane taken in the cockpit

5. **Air velocity around the cockpit:** In this criterion, gasper configuration has an advantage of adjustability. Therefore, even the velocities are seen too high or low at the cockpit, flow rate and the direction of the gaspers can be changed and pilot can provide herself/himself suitable conditions. Streamline of velocity contour is given in Figure 3.3-6 for gasper configuration.

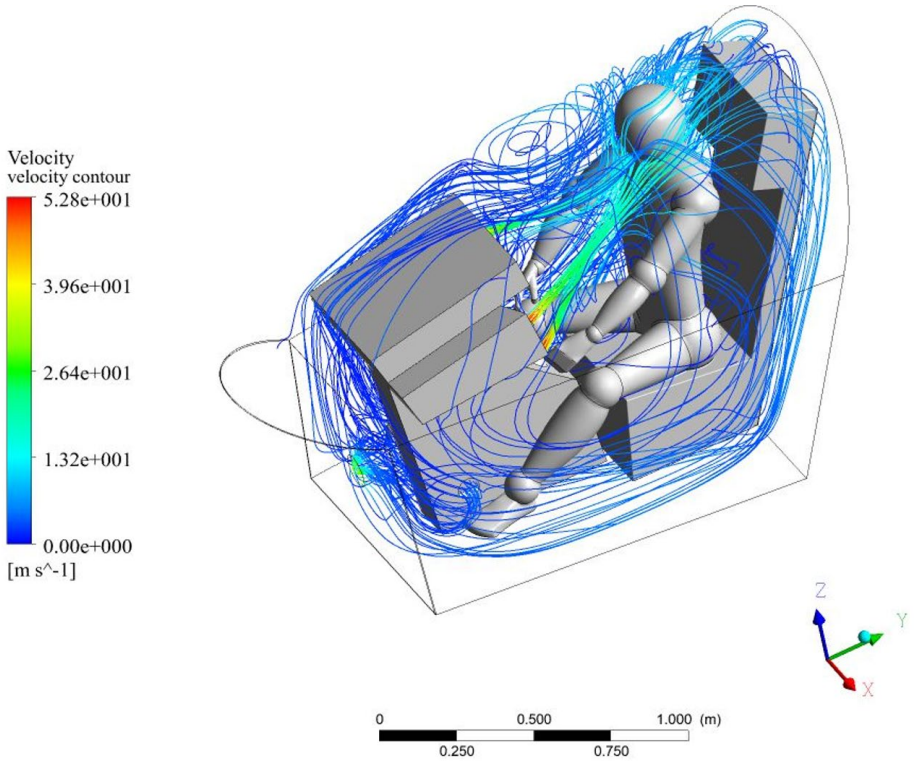

Figure 3.3-6 3D velocity magnitude streamline contour around the cockpit with gasper inlets

Two different velocity magnitude planes have been created to compare the two configurations clearly in Figure 3.3-7 and Figure 3.3-8. According to these contours, velocities are higher in the gasper case, which provides well-distributed air around the cockpit. In addition, velocities are higher around the pilot in the gasper case providing better cooling to the occupant.

(a)

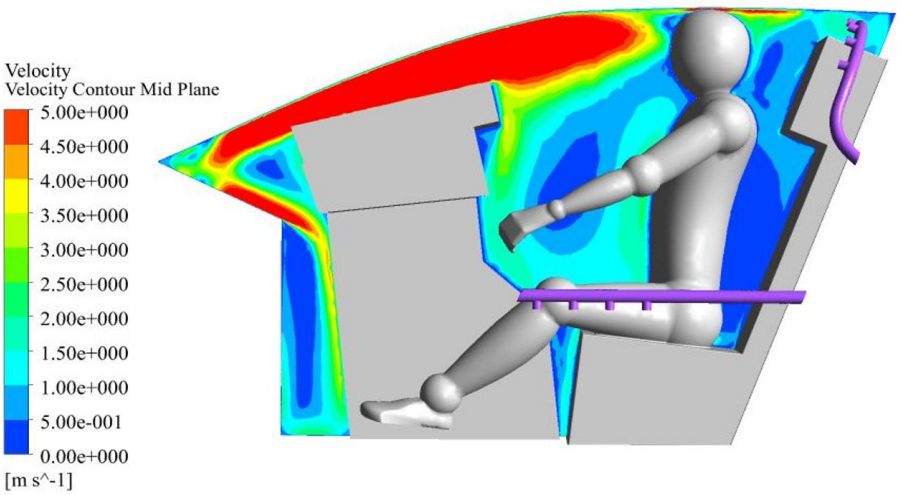

(b)

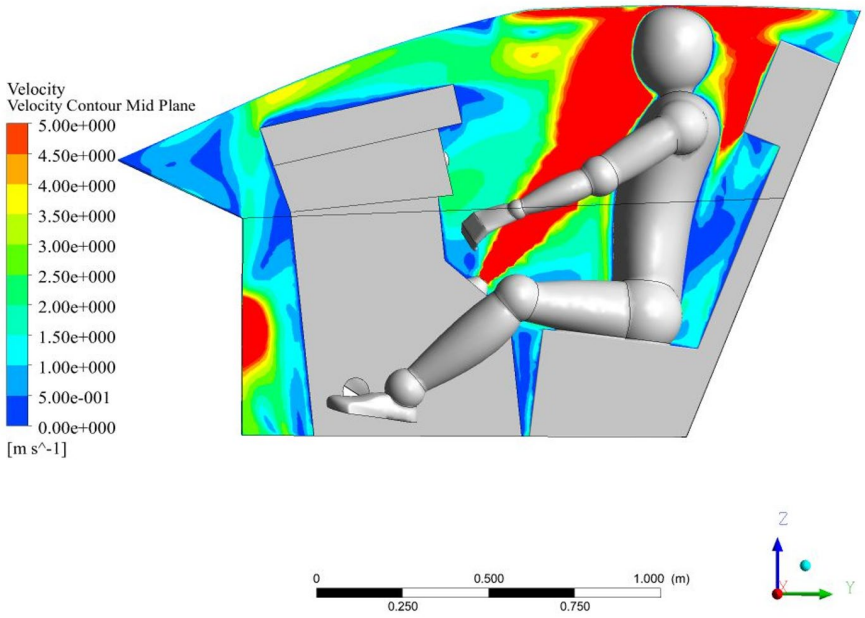

Figure 3.3-7 (a) Velocity magnitude contour of piccolo inlet (b) Velocity magnitude of gasper inlet from middle plane taken in the cockpit

(a)

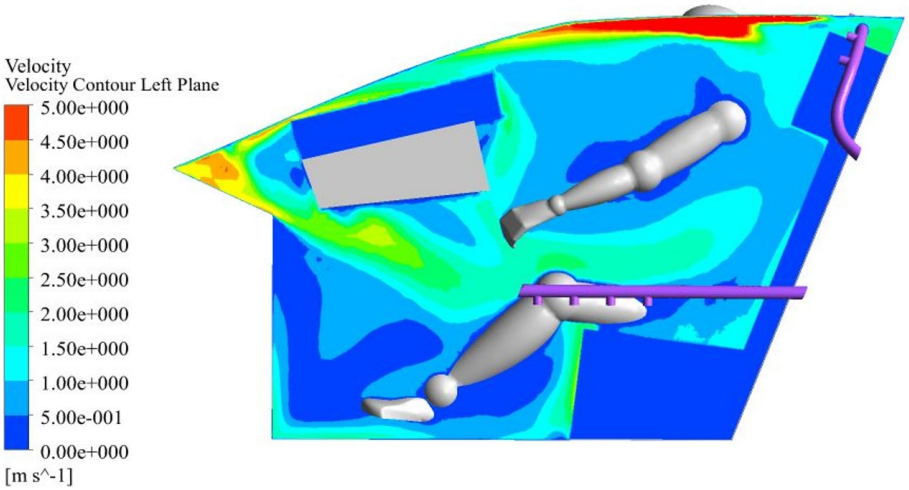

(b)

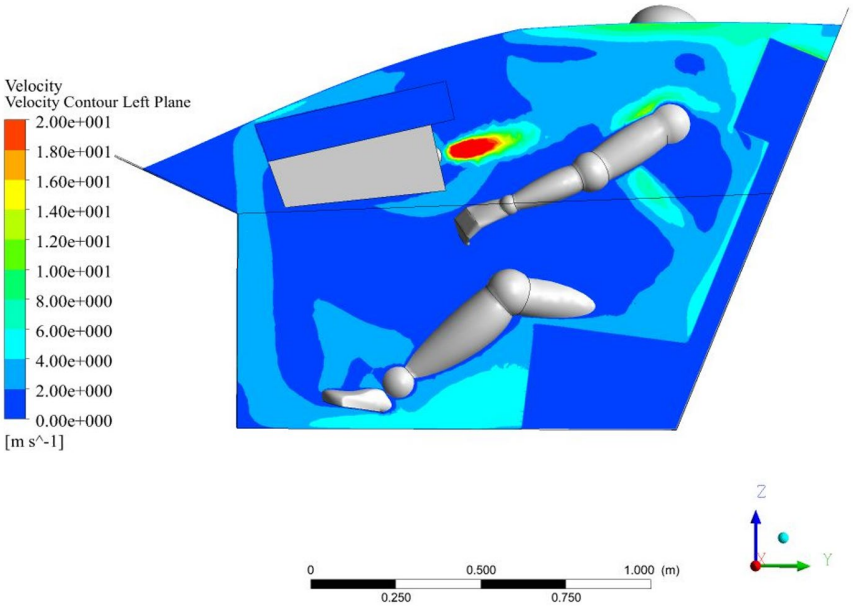

Figure 3.3-8 (a) Velocity magnitude contour of piccolo inlet (b) Velocity magnitude of gasper inlet from left plane taken in the cockpit

6. **Exhaust Air Temperature:** When both case outlet temperatures are evaluated, no critical differences are detected, as given in Table 4-2. As in Section 3.3, the gasper configuration also meets the criteria defined in the standards.

Table 4-2 Outlet Temperature and Velocity values for both configurations

Cooling Outlet Configuration	Average Outlet Temperature (°C)	Average Outlet Velocity (m/s)
Piccolo	26.69	9.2
Gasper	26.63	17.7

The next step, which is calculating the pilot envelope temperature, will not give a precise thermal comfort evaluation because of the almost same outlet temperatures. Therefore, a WBGT calculation has been done for the comparison of these two configurations.

The Globe temperature, clothing effect and the metabolic rate are same for the both configurations since the cockpit and the pilot are same in both configurations. Therefore, effects of these factors have been added directly. According to these inputs, temperature around the head and shoulder have been measured for the WBGT for gasper configuration in Table 4-3. As a result of the values, gasper configuration stayed at much lower values than piccolo configuration.

Table 4-3 Resultant WBGT measurements from different part of the human body for gasper inlets

	DBT (°C)	WBT (°C)	GT (°C)	WBGT (°C)	WBGT (°F)	Resultant WBGT with clothing effect (°F)
Head	26	12.17	56.122	22.34	72.22	82.22
Shoulder	24	10.88	56.122	21.24	70.24	80.24

All in all, when both cases have been compared, gasper configuration gave better results than piccolo configuration as given in Table 4-4.

Table 4-4 Comparison of Thermal Comfort Evaluation Parameters

No	Thermal Comfort Evaluation Parameters	Piccolo	Gasper	Criteria
1	The number of inlets	16	5	Minimum 2
2	The position of the inlets	Directed to cockpit interior	Directed to pilot	Directed to pilot
3	Supply air temperature	4°C	4°C	At least 2°C
4	Temperature difference between the head and foot of the pilot	~6°C	~3°C	Maximum 2.8°C
5	Air velocity around the cockpit	Refer to Figure 3.3-7 and Figure 3.3-8	Refer to Figure 3.3-7 and Figure 3.3-8	Higher than 1 m/s around the pilot
6	Exhaust Air Temperature	26.69 °C	26.63°C	Maximum 35°C
7	Wet Bulb Globe Temperature	Head: 84.19 °F Shoulder: 90.15 °F	Head: 82.22 °F Shoulder: 80.24 °F	Maximum 90°F For ground operations

CHAPTER 5

CONCLUSION

In this thesis, thermal comfort investigation has been done for one-seated military aircraft cockpit with the help of computational fluid dynamics. Thermal comfort factors have been detailly studied and different kind of inlets have been reviewed. Two different inlet types of piccolo and gasper have been compared. For the comparison of these two inlets, different kinds of parameters have been defined as given in Table 4-4. Since the standard suggestions are not only enough for the thermal comfort evaluations, two different thermal comfort measurement indices have been used to investigate the factor effect on human comfort.

As a result of these evaluations, it is concluded that:

- The temperature difference between head and foot is essential to understand that the air distribution around the pilot is at enough levels.
- Jet air provided to the cockpit provides well-distributed air inside the cockpit.
- Foot inlets have an important role for the air-distribution in the cockpit.
- The temperatures taken from the inlet and the outlet of the cockpit are not enough to evaluate the thermal comfort of the occupant.
- The pilot's clothing significantly affects the thermal comfort because of the well-insulated form of their clothes.
- Wet Bulb Globe Temperature index is an efficient method for thermal comfort calculations.

In addition to thermal observations, there are also numerical observations have been taken from this study:

- Solving unsteady problem with steady solver does not give smooth results. For the precise studies, unsteady solver should be tried.

- Inflation layer has a great role over the y+ quality for the enhanced wall treatment property of ANSYS Fluent. It should cover the Boundary Layer and not distort the mesh quality.
- With the increasing complexity of the geometry, meshing quality becomes more important.

For the further studies, below items can be done to improve and understand the thermal comfort issues:

- Unsteady solver can be used to improve the solution convergencies.
- Human model can be separated into different heat transfer rates as given in Table 1.3.1-1.
- Another detailed thermal comfort measurement index which is PMV defined in Section 1.4.3.3 can be used to understand the pilot is at satisfied conditions.
- k-ω turbulence model can be used to review for the convergency of the model without adding any inflation layer.
- Different configurations of gasper and piccolo case can be tried. For instance,
    - Outlet can be installed over front bulkhead and foot inlet can be added for the piccolo case
    - Outlet can be installed over the rear bulkhead and two of the gasper inlets can be installed over the side panels for the gasper case
- Two-phase modelling can be done to understand the water vapor effect on thermal comfort.
- Complexity of the geometry can be increased with actual cockpit configuration.

REFERENCES

1 Wu, Y., Liu, H., Li, B., Cheng, Y., Tan, D., & Fang, Z. (2017). Thermal comfort criteria for personal air supply in aircraft cabins in winter. *Building and Environment*, *125*, 373–382.

2 Konstantinov, M., Lautenschlager, W., Shishkin, A., & Wagner, C. (2014). Numerical Simulation of the Air Flow and Thermal Comfort in Aircraft Cabins. *German Aerospace Center, Institute of Aerodynamics and Flow Technology*.

3 Yuan, X. (2011). The Application of the Human Model in the Thermal Comfort Assessment of Fighter Plane's Cockpit. *Digital Human Modeling*, 357–366.

4 Liu, W., Wen, J., Lin, C.-H., Liu, J., Long, Z., & Chen, Q. (2013). Evaluation of various categories of turbulence models for predicting air distribution in an airliner cabin. *Building and Environment*, 65, 118–131.

5 Liu, W., Mazumdar, S., Zhang, Z., Poussou, S. B., Liu, J., Lin, C.-H., & Chen, Q. (2012). State-of-the-art methods for studying air distributions in commercial airliner cabins. *Building and Environment*, 47, 5–12.

6 Ningbai, N. (2014). *Analysis of Air Flow Distribution and Thermal Comfort in Hybrid Electric Vehicles.* [M.Sc. Thesis] Simon Fraser University.

7 Liu, W., Duan, R., Chen, C., Lin, C.-H., & Chen, Q. (2015). Inverse design of the thermal environment in an airliner cabin by use of the CFD-based adjoint method. *Energy and Buildings*, 104, 147–155.

8 Johansson, E. (2017). *The thermal comfort of the cockpit: A pilot's experience*. [M.Sc. Thesis] KTH Royal Institute of Technology School of Engineering Science.

9 Pang, L., Li, P., Bai, L., Liu, D., Zhou, Y., & Yao, J. (2018). Optimization of air distribution mode coupled interior design for civil aircraft cabin. *Building and Environment*, 134, 131–145.

10 Şahin, D. (2018). *Analysis of Flow Structure in a Helicopter Cabin to Improve the Thermal Comfort Using Computational Fluid Dynamics Modeling.* [M.Sc. Thesis] Middle East Technical University.

11 Jia, Z., Wang, Q., Zeya, A., Sun, Z., & Zhao, Y. (2019). Optimal Design of the Flow Field Control in a Cockpit. *Lecture Notes in Electrical Engineering*, 709–717.

12 Kotb, H., & Khalil, E. E. (2020). Passengers' Thermal Comfort in Wide-Body Aircraft Cabin. *AIAA Propulsion and Energy 2020 Forum*.

13 Hassan, M. T., Yu, J., Zhu, W., Liu, F., Liu, J., & An, N. (2018). Monitoring Thermal Comfort with IoT Technologies: A Pilot Study in Chinese Eldercare Centers. *Human Aspects of IT for the Aged Population. Applications in Health, Assistance, and Entertainment*, 303–314.

14 ASHRAE. (2019). *Standard 55 – Thermal Environmental Conditions for Human Occupancy.*

15 Mathis, P., Streblow, R., Grün, G., Wick, A., & Thalabart, J.-C. (2011). Thermal Comfort Simulation in Modern Aircraft Cockpits. In *publications.rwth-aachen.de*. Tapir Akademisk Forlag. https://publications.rwth-aachen.de/record/118218

16 Chrenko, F. A. (1967). Paper 8: Thermal Comfort. *Proceedings of the Institution of Mechanical Engineers, Conference Proceedings*, 182(5), 13–19.

17 JSSG 2009: *Military Specification Environmental Control Systems, Aircraft General Requirements*

18 MIL-E-18927E: *Military Specification Environmental Control Systems, Aircraft General Requirements*

19 SAE International, SAE-ARP-85F: *Air-Conditioning Systems for Subsonic Airplanes*

20 DEF-STAN 00-970 *Section 4: Ministry of Defense-Defense Standard*

21 Stribley, R. F.; Nunneley, S.A. (1978) Fighter Index of Thermal Stress: Development of Interim Guidance for Hot-Weater USAF Operations. *USAF School of Aerospace Medicine*.

22 Joint Base Myer-Henderson Hall Safety Office. (2014, July). *U.S. ARMY*. Retrieved from: https://www.army.mil/article/129507/joint_base_myer_henderson_hall_wet_bulb_globe_temperature

23 Hughes, T. (1968). Cabin Air Requirements for Crew Comfort in Military Aircraft. *Aeronautical Research Council. London: Ministry of Technology*.

24 Boussinesq, J. (1872). *Essai Sur La Theorie Des Eaux Courantes.* Paris.

25 Schlichting, H. (1979). *Boundary Layer Theory*, [7th ed.]

26 ANSYS, Inc, *Ansys Fluent Theory Guide 15.0, 2013*

27 You, R., Chen, J., Shi, Z., Liu, W., Lin, C.-H., Wei, D., and Chen, Q. 2016. *Experimental and numerical study of airflow distribution in an aircraft cabin mockup with a gasper on*. Building Performance Simulation, 9(5): pp. 555-566.

28 Danca, P., Coşoiu, C., Nastase, I., Bonde, F., & Georgescu, M. R. (2022). Personalized Ventilation as a Possible Strategy for Reducing Airborne Infectious Disease Transmission on Commercial Aircraft. *Applied Sciences,* 12 (4), 2088.

29 Malalasekera, W., & Versteeg, H. (2007). *An Introduction to Computational Fluid Dynamics, The Finite Volume Method.* [2nd ed.] Pearson.

30 *Module 3: Global Mesh Controls Introduction to ANSYS Meshing*. (n.d.). https://drahmednagib.com/CAD_2018/Lecture_3_Meshing_2.pdf

31 NATO: Military Agency for Standardization- STANAG 2895 MMS (EDITION 1) - Extreme Climatic Conditions and Derived Conditions for Use in Defining Design/Test Criteria for Nato Forces Materiel

32 Psikuta, A., Allegrini, J., Koelblen, B., Bogdan, A., Annaheim, S., Martínez, N., Derome, D., Carmeliet, J., & Rossi, R. M. (2017). Thermal manikins controlled by human thermoregulation models for energy

efficiency and thermal comfort research – A review. *Renewable and Sustainable Energy Reviews*, 78, 1315–1330.

33 Sørensen, D. N., & Voigt, L. K. (2003). Modelling flow and heat transfer around a seated human body by computational fluid dynamics. *Building and Environment*, 38(6), 753–762.

34 S. H. N Turco, T. G. F da Silva, G M de Oliveira, M. M. V. B. R Leitão, M. S. B de Moura, C Pinheiro, & C. V da Silva Padilha. (2008). Estimating Black Globe Temperature Based on Meteorological Data. *Livestock Environment VIII, 31 August - 4 September 2008, Iguassu Falls, Brazil.*

35 Ducharme, M. (2006). *Thermal insulation of the LASA ventilated-NBC suit during immersion in cold water.*

36 Rebbechi, B. (1980). *A review of aircraft cabin conditioning for operations in Australia, Department of Defense*. Melbourne: Aeronautical Research Labs.

37 Launder, B. E. and Spalding, D. B. (1972). *Lectures in Mathematical Models of Turbulence*. Academic Press, London, England.